PFC/JA-83-9

PARAMETRIC EXCITATION OF ION-SOUND QUASI-MODES DURING LOWER HYBRID HEATING EXPERIMENTS IN TOKAMAKS

Y. Takase and M. Porkolab

Plasma Fusion Center
Massachusetts Institute of Technology
Cambridge, MA 02139

February 1983

This work was supported by the U.S. Department of Energy Contract No. DE-AC02-78ET51013. Reproduction, translation, publication, use and disposal, in whole or in part by or for the United States government is permitted.

By acceptance of this article, the publisher and/or recipient acknowledges the U.S. Government's right to retain a non-exclusive, royalty-free license in and to any copyright covering this paper.

PARAMETRIC EXCITATION OF ION-SOUND QUASI-MODES DURING LOWER HYBRID HEATING EXPERIMENTS IN TOKAMAKS

Y. Takase and M. Porkolab

Department of Physics and Plasma Fusion Center,

Massachusetts Institute of Technology,

Cambridge, Massachusetts 02139

Parametric decay of a lower hybrid pump wave into another lower hybrid wave and a low frequency ion-sound quasi-mode ($\omega_R \simeq k_{\|} v_{ti}$) is studied. Such an instability may be excited during high-power lower hybrid heating experiments in tokamak plasmas and may lead to strong modification of the incident $n_{\|}$ spectrum near the plasma periphery. Such an instability could explain the broadened and downshifted frequency spectrum and phase-independent heating observed in the Alcator A tokamak experiments. Although the growth rate for this decay increases like $\gamma + \Gamma_2 \sim E_0^2$ for powers slightly above threshold (Γ_2 is the linear damping rate at the lower sideband and E_0 is the pump electric field), for powers well above threshold (such that $\gamma \gtrsim \omega_R$) $\gamma \sim E_0^{2/3}$, and the convective thresholds are rather high. However, for inaccessible $n_{0\|}$, the pump wave power is expected to accumulate on the outer surface of the plasma column where the growth rate is large and the convective thresholds are significantly reduced. In such a case the threshold pump power can become quite low and may be exceeded in experiments such as Alcator A.

I. INTRODUCTION

During the Alcator A lower hybrid heating experiments, frequency downshifted and broadened RF spectrum and enhanced low frequency spectrum were observed on RF probes located in the shadow of the limiter.[1] Frequency downshifted and broadened RF spectrum was also observed in the plasma interior using small angle CO_2 laser scattering.[2] Similar frequency spectra have been observed in Alcator C with both RF probes[3] and CO_2 scattering.[4] In addition, the ion tail production observed in Alcator A was found to be independent of waveguide phasing.[1]

One possible explanation of these results is the scattering of lower hybrid waves at the plasma edge by the low frequency density fluctuations. [2,5,6] While this mechanism accounts for many of the observed features in the Alcator A experiment, it cannot easily explain the downshifted RF frequency spectrum and the enhanced low frequency spectrum. In addition, it would take hundreds of scattering events to explain the broad (up to 8MHz FWHM) frequency spectrum observed. In this paper, we consider another process, namely the parametric decay of the lower hybrid pump wave, $\omega_0 = \omega_{LH}[1 + (m_i/m_e)(k_\parallel^2/k^2)]^{1/2}$, into another lower hybrid wave and a low frequency ion-sound quasi-mode, $\omega_R \simeq k_\parallel v_{ti}$ (ω_R/ω_0 is typically of the order of 10^{-3}). Through this parametric decay, higher $n_\parallel$ lower hybrid waves can be generated. We find that for the accessible part of the $n_{0\parallel}$ spectrum, due to the narrow resonance cones the convective thresholds are rather high ($P \gtrsim$1MW). However, the inaccessible components of the pump wave spectrum will accumulate on the outer surface of the plasma column where the growth rates for this parametric process is high. If the parametrically excited sideband waves propagate mainly in the poloidal direction (as opposed to the radial direction) the threshold can be low ($P \lesssim$ 1kW) compared with the available pump power. Therefore, we would expect that this process might play an important role in experiments where a significant fraction of the incident power is in the inaccessible range of $n_{0\|}$. In this paper we shall not consider the effects of scattering from density fluctuations or toroidal geometry. We remark, however, that toroidal effects may also produce a pump wave that propagates to the surface periodically.[5]

The plan of the paper is as follows: In Section II, analytical and numerical calculations of homogeneous growth rates and thresholds are presented. In Sections III – V, various convective and inhomogeneous thresholds are estimated. The depletion of the pump wave due to this decay instability is discussed in Section VI. Finally, in Section VII the summary and conclusions are given.

II. HOMOGENEOUS GROWTH RATES AND THRESHOLDS

We consider here only the outer region of the plasma column, namely $r/a \gtrsim 0.75$ where a is the limiter radius. We consider the slab geometry shown in Fig. 1. Here, x, y and z correspond to the radial, the poloidal and the toroidal direction, respectively, in a torus. We assume an RF pump wave of the form

$$\mathbf{E}_0 = (\mathbf{E}_{0\|} + \mathbf{E}_{0\perp})\cos(\omega_0 t - \mathbf{k}_0 \cdot \mathbf{x})$$

where $\mathbf{E}_{0\|}$ is the component of $\mathbf{E}_0$ in the z-direction and $\mathbf{E}_{0\perp}$ is the component of $\mathbf{E}_0$ perpendicular to the external magnetic field (which need not be in the x-direction). Near the plasma edge, we shall not distinguish between the z- and the parallel direction $\mathbf{B}/B$.

We use the parametric dispersion relation derived by Porkolab[7]:

$$\begin{aligned}1+\frac{1}{\chi_i} = {} & J_0{}^2(\mu)\frac{\chi_e}{1+\chi_e} + J_1{}^2(\mu)\left(\frac{\chi_e^+}{1+\chi_e^+}+\frac{\chi_e^-}{1+\chi_e^-}\right)\\ & + \frac{J_0{}^2(\mu)J_1{}^2(\mu)\left[\dfrac{\chi_e}{1+\chi_e}-\dfrac{\chi_e^+}{1+\chi_e^+}\right]}{1+\dfrac{1}{\chi_i^+}-J_0{}^2(\mu)\dfrac{\chi_e^+}{1+\chi_e^+}-J_1{}^2(\mu)\dfrac{\chi_e}{1+\chi_e}}\\ & + \frac{J_0{}^2(\mu)J_1{}^2(\mu)\left[\dfrac{\chi_e}{1+\chi_e}-\dfrac{\chi_e^-}{1+\chi_e^-}\right]}{1+\dfrac{1}{\chi_i^-}-J_0{}^2(\mu)\dfrac{\chi_e^-}{1+\chi_e^-}-J_1{}^2(\mu)\dfrac{\chi_e}{1+\chi_e}}\end{aligned} \tag{1}$$

where $\chi_{i,e} \equiv \chi_{i,e}(\omega, \mathbf{k})$ and $\chi_{i,e}^{\pm} \equiv \chi_{i,e}(\omega^{\pm}, \mathbf{k}^{\pm})$ are the linear susceptibilities at the low frequency (ω,$\mathbf{k}$) and at the sidebands ($\omega^{\pm} \equiv \omega \pm \omega_0$, $\mathbf{k}^{\pm} \equiv \mathbf{k} \pm \mathbf{k}_0$) respectively, and J's are the Bessel functions. We used the following expressions for the susceptibilities in our numerical calculations:

$$\chi_e(\omega,\mathbf{k}) \simeq \frac{1}{k^2\lambda_{De}^2}\frac{\left[1+\dfrac{\omega-\omega_{*e}+i\nu_e}{k_\parallel v_{te}}I_0(b_e)e^{-b_e}Z\left(\dfrac{\omega+i\nu_e}{k_\parallel v_{te}}\right)\right]}{\left[1+\dfrac{i\nu_e}{k_\parallel v_{te}}I_0(b_e)e^{-b_e}Z\left(\dfrac{\omega+i\nu_e}{k_\parallel v_{te}}\right)\right]}, \tag{2}$$

$$\chi_i(\omega,\mathbf{k}) \simeq \frac{1}{k^2\lambda_{Di}^2}\left[1+\frac{\omega-\omega_{*i}}{k_\parallel v_{ti}}\sum_{n=-100}^{100} I_n(b_i)e^{-b_i}Z\left(\frac{\omega-n\Omega_i}{k_\parallel v_{ti}}\right)\right]. \tag{3}$$

Here, $v_{ti,e} \equiv (2T_{i,e}/m_{i,e})^{1/2}$, $\Omega_{i,e} \equiv \pm\omega_{ci,e} \equiv \pm eB/m_{i,e}c$, $b_{i,e} \equiv k_\perp^2 v_{ti,e}^2/2\Omega_{i,e}^2$, I's are the modified Bessel functions, Z is the Fried-Conte plasma dispersion function, and ν_e is the effective electron collision frequency which includes electron-ion and electron-neutral collisions. We have included the effects of drift waves in the susceptibilities by introducing the drift frequencies $\omega_{*i,e} \equiv k_y v_{ti,e}^2/2\Omega_{i,e}L_n$ where $L_n \equiv n|dn/dx|^{-1}$.

In the dipole approximation ($\mathbf{k}_0 = 0$), the coupling constant μ is given by[7]

$$\mu \simeq \frac{e}{m_e}\left[\frac{k_\parallel^2 E_{0\parallel}^2}{\omega_0^4} + \frac{[(\mathbf{E}_{0\perp}\times\mathbf{k}_\perp)\cdot\hat{z}]^2}{\omega_0^2\omega_{ce}^2}\right]^{\frac{1}{2}}$$

where $\hat{z}$ is the unit vector in the z-direction. We have neglected the polarization drift term but kept the parallel electron drift term and the $\mathbf{E}\times\mathbf{B}$ term which are important near the edge. For finite $\mathbf{k}_0$, we have to use different expressions for μ at upper and lower sidebands (μ^+ and μ^-). Following Drake *et al*,[8] we obtain the following dispersion relation:

$$\epsilon + \frac{1}{4}\left[\frac{(\mu^-)^2}{\epsilon^-} + \frac{(\mu^+)^2}{\epsilon^+}\right]\chi_e(1+\chi_i) = 0 \tag{4}$$

where

$$\mu^\pm \simeq \frac{e}{m_e}\frac{k}{k^\pm}\left[\frac{\left(k_\parallel^\pm\right)^2 E_{0\parallel}^2}{\omega_0^4} + \frac{\left[\left(\mathbf{E}_{0\perp}\times\mathbf{k}_\perp^\pm\right)\cdot\hat{z}\right]^2}{\omega_0^2\omega_{ce}^2}\right]^{\frac{1}{2}}. \tag{5}$$

We remark that Eq. (4) is valid only if $\mu^2 \ll 1$ whereas Eq. (1) is valid even near $\mu \simeq 1$ (but $k_0/k \ll 1$). Thus, Eqs. (1) and (4) may be used to explore somewhat different regimes.

In the limit $\mu^2 \ll 1$ we can expand the Bessel functions in Eq. (1) and we arrive at the well-known parametric dispersion relation[7]

$$\epsilon + \frac{1}{4}\left[\frac{\mu^2}{\epsilon^-} + \frac{\mu^2}{\epsilon^+}\right](1+\chi_e)\chi_i = 0. \tag{6}$$

We note that the contribution from the upper sideband can be neglected if $|\epsilon^+| \gg |\epsilon^-|$. In this case, we may neglect the second term in the bracket in Eqs. (4) and (6) and the two expressions agree provided that we use μ^- for μ at the lower sideband in Eq. (6) and provided that $\chi_{eR} \gg 1$ and $\chi_{iR} \gg 1$. Here, $\Gamma_2 \equiv \epsilon_I(\omega_2)/(\partial\epsilon_R/\partial\omega_2)$ is the linear damping rate at the lower sideband $\omega_2 \simeq \omega_0 - \omega$.

II-A. ANALYTIC CALCULATIONS

Near the edge of a tokamak plasma where $T_e \simeq T_i$, we shall consider parametric decay into low frequency ion-sound quasi-modes such that $\omega_R \simeq k_{||}v_{ti} \ll k_{||}v_{te}$. Furthermore, since at the waveguide mouth the plasma is mildly overdense, we assume that at the edge region $\omega_{pe} > |\omega^-| \gg \omega_{pi}$ (where $\omega^- \equiv \omega - \omega_0$). Neglecting the upper sideband, from Eq. (6) we get

$$1 + \frac{\mu^2}{4}\frac{\chi_i\chi_e}{\epsilon\epsilon^-} \simeq 0 \tag{7}$$

where we have assumed that $|\chi_{eR}| \gg 1$. On the other hand, from Eq. (4) we get

$$1 + \frac{(\mu^-)^2}{4}\frac{\chi_e\chi_i}{\epsilon\epsilon^-} \simeq 0 \tag{8}$$

where we have assumed $|\chi_{iR}| \gg 1$.

For powers slightly above threshold so that $\gamma \ll \omega_R$, we find from our numerical studies that the following approximations hold: $|\chi_{eR}| \gg |\chi_{iR}|$, $|\chi_{iI}| \gg |\chi_{eI}|$, and $|\chi_{iI}| \lesssim |\chi_{eR}|$. Taking the imaginary part of either Eq. (7) or Eq. (8) then gives

$$(\gamma + \Gamma_2)\frac{\partial \epsilon_R}{\partial \omega_2} \simeq \frac{(\mu^-)^2}{4} \frac{\chi_{iI}\chi_{eR}^2}{\chi_{eR}^2 + \chi_{iI}^2}$$

where $\epsilon_R(\omega_2) = 0$, *i.e.*, $\omega_2 = \omega_{LH}[1 + (m_i/m_e)(k_{2\|}/k_2)^2]^{1/2}$, $\Gamma_2 \simeq (\nu_e/2)(1 - \omega_{LH}^2/\omega_2^2 + \omega_{LH}^2/\omega_{ce}\omega_{ci})$, and we have used μ^- for μ. We get the following expression for the growth rate:

$$\frac{\gamma + \Gamma_2}{\omega_2} \simeq \frac{(\mu^-)^2}{8}\left(1 + \frac{\omega_{pe}^2}{\omega_{ce}^2}\right)^{-1} \frac{F}{k^2\lambda_{Di}^2} \tag{9}$$

where

$$F \equiv \frac{\pi^{1/2}\,\varsigma_{0i}\exp\left(-\varsigma_{0i}^2\right)}{1 + \left(\dfrac{T_e}{T_i}\right)^2 \pi\,\varsigma_{0i}^2 \exp\left(-2\,\varsigma_{0i}^2\right)}; \qquad \varsigma_{0i} \equiv \frac{\omega}{k_\| v_{ti}}.$$

We see that the growth rate increases like $\gamma + \Gamma_2 \sim E_0^2$ for powers just above threshold.

However, for powers well above threshold such that $\gamma \gtrsim \omega_R \gg k_\| v_{ti}$, χ_i can be expanded as

$$\begin{aligned}\chi_i &\simeq \frac{1}{k^2\lambda_{Di}^2}\left[1 - (1 + \frac{1}{2\varsigma_{0i}^2} + \frac{3}{4\varsigma_{0i}^4} + \cdots)\right] - \frac{k_\perp^2}{k^2}\frac{\omega_{pi}^2}{\omega^2 - \omega_{ci}^2} \\ &\simeq -\frac{k_\|^2}{k^2}\frac{\omega_{pi}^2}{\omega^2}\left[1 + \frac{3}{2}\frac{k_\|^2 v_{ti}^2}{\omega^2} + \cdots\right]\end{aligned}$$

since the perpendicular component of the ion susceptibility is usually negligibly small in the outer plasma layers. For sufficiently large $\omega_R/k_\| v_{ti}$ and $\gamma/k_\| v_{ti}$ we have $|\chi_{eR}| \gg |\chi_{iR}|$ and $|\chi_{eI}| \gg |\chi_{iI}|$, in which case we get

$$\frac{\partial \epsilon_R}{\partial \omega_2}[(\omega_R - \delta) + i(\gamma + \Gamma_2)] \simeq \frac{(\mu^-)^2}{4}\chi_i$$

where $\delta \equiv \omega_0 - \omega_2$. Solving the real and imaginary parts simultaneously and maximizing the growth rate with respect to δ gives

$$\frac{\omega_R}{\omega_0} \simeq \frac{1}{4}\left[(\mu^-)^2 \frac{k_\parallel^2}{k^2}\frac{\omega_{LH}^2}{\omega_0^2}\right]^{\frac{1}{3}} \tag{10}$$

$$\frac{\gamma}{\omega_0} \simeq \frac{3^{1/2}}{4}\left[(\mu^-)^2 \frac{k_\parallel^2}{k^2}\frac{\omega_{LH}^2}{\omega_0^2}\right]^{\frac{1}{3}} = 3^{1/2}\,\frac{\omega_R}{\omega_0} \tag{11}$$

and $\delta = 0$, where the approximation $\Gamma_2 \ll \gamma$ has been used. We see that the growth rate increases only like $\gamma \sim E_0^{2/3}$. This is similar to the fluid quasi-mode discussed by Porkolab.[7] In this paper we shall refer to this as the reactive quasi-mode. Our numerical solutions often follow this power scaling. However, the ion-sound quasi-mode decay tends to get overshadowed by the ion-cyclotron quasi-mode decay at high pump powers when γ/ω_{ci} approaches 1. In Fig. 2 we show the comparison between the analytic scaling given by Eqs. (10) and (11) (solid curves) and the numerical solutions of the more complete dispersion relation Eq. (1). We see that the agreement between the two techniques is good.

The transition from decay into dissipative quasi-modes to that into reactive quasi-modes occurs for $\gamma \gtrsim \omega_R \gtrsim 2k_\parallel v_{ti}$ as can be seen from Fig. 3. Here, we show a contour plot of $\log_{10}|\chi_{iIm}/\chi_{eIm}|$ as a function of $\omega_R/k_\parallel v_{ti}$ and $\gamma/k_\parallel v_{ti}$. The following parameters were used for this plot: Alcator A, deuterium plasma, $B = 5\text{T}$, $n_e = 1 \times 10^{12}\text{cm}^{-3}$, $T_e = T_i = 3\text{eV}$, $ck_{0\parallel}/\omega_0 = 2$ and $ck_\parallel/\omega_0 = 7$.

The ratio of the $E_\parallel$ coupling term to the $\mathbf{E} \times \mathbf{B}$ coupling term in $(\mu^-)^2$ is given by[9]

$$\frac{\left(\dfrac{k_{2\|}E_{0\|}}{\omega_0}\right)^2}{\left[\dfrac{(\mathbf{E}_{0\perp}\times\mathbf{k}_{2\perp})\cdot\hat{z}}{\omega_{ce}}\right]^2}\simeq\frac{k_{0\|}^4\omega_{ce}^2}{k_{0\perp}^4\omega_0^2}\simeq\frac{\omega_0^2\omega_{ce}^2}{\omega_{pe}^4} \tag{12}$$

where we have assumed $E_{0\|}/E_{0\perp}\simeq k_{0\|}/k_{0\perp}\simeq k_{0\|}/k_0\simeq\omega_0/\omega_{pe}$, $k_{2\|}/k_2\simeq k_{2\|}/k_{2\perp}\simeq k_{0\|}/k_{0\perp}$, and $\mathbf{k}_{0\perp}\perp\mathbf{k}_{2\perp}$. We see that the $E_{\|}$ coupling term dominates if $\omega_{pe}^2<\omega_0\omega_{ce}$, and the $\mathbf{E}\times\mathbf{B}$ coupling dominates in the opposite case. For typical Alcator A edge conditions of $B=5$T and $f_0=2.45$GHz, $E_{\|}$ coupling dominates in the growth rate for densities $n_e<4.2\times10^{12}\text{cm}^{-3}$.

We now consider powers just above threshold. When $E_{\|}$ coupling dominates, we can drop the $\mathbf{E}\times\mathbf{B}$ coupling term in μ^- and from Eq. (9) we get the following expression for the growth rate:

$$\frac{\gamma+\Gamma_2}{\omega_0}\simeq\frac{F}{4}\frac{v_{D\|}^2}{v_{te}^2}\frac{T_e}{T_i}, \tag{13}$$

where $v_{D\|}\equiv eE_{0\|}/m_e\omega_0$, and the approximations $\omega_{pe}^2\ll\omega_{ce}^2$ and $\omega_{pi}^2\ll\omega_0^2$ were used. In a uniform plasma the threshold can be obtained from Eq. (13) by setting $\gamma=0$:

$$E_{0\|}^2\simeq\frac{m_e^2\omega_0^2}{e^2}\frac{4}{F}\frac{T_i}{m_e}\frac{\nu_e}{\omega_0}. \tag{14}$$

Similarly, if $\mathbf{E}\times\mathbf{B}$ coupling dominates over $E_{\|}$ coupling, we get for the growth rate

$$\frac{\gamma+\Gamma_2}{\omega_0}\simeq\frac{F}{4}\left(\frac{\mathbf{k}_{0\perp}\times\mathbf{k}_{2\perp}}{k_0k_2}\right)^2\frac{\omega_{LH}^2}{\omega_0^2}\frac{U^2}{v_{ti}^2},$$

where $U\equiv cE_{0\perp}/B$. For the uniform plasma threshold we get

$$E_{0\perp}^2\simeq\frac{B^2}{c^2}\frac{\omega_0^2}{\omega_{LH}^2}\frac{4}{F}\frac{T_i}{m_i}\frac{\nu_e}{\omega_0}\left(1-\frac{\omega_{LH}^2}{\omega_0^2}+\frac{\omega_{LH}^2}{\omega_{ce}\omega_{ci}}\right)\left(\frac{k_0k_2}{\mathbf{k}_{0\perp}\times\mathbf{k}_{2\perp}}\right)^2.$$

For powers well above threshold we get from Eq. (11) for the $E_{||}$ dominated case

$$\frac{\gamma}{\omega_0} \simeq \frac{3^{1/2}}{4}\left[\frac{m_e}{m_i}\frac{k_{||}^2 v_{D||}^2}{\omega_0^2}\right]^{\frac{1}{3}} \tag{15}$$

and for $\mathbf{E} \times \mathbf{B}$ dominated case

$$\frac{\gamma}{\omega_0} \simeq \frac{3^{1/2}}{4}\left[\left(\frac{\mathbf{k}_{0\perp} \times \mathbf{k}_{2\perp}}{k_0 k_2}\right)^2 \frac{\omega_{LH}^2}{\omega_0^2}\frac{k_{||}^2 U^2}{\omega_0^2}\right]^{\frac{1}{3}}. \tag{16}$$

Typical threshold values are given in Table I. For the Alcator A experiment, $E_{0||} = 330\text{V/cm}$ at the waveguide mouth roughly corresponds to a total incident power of $P_{RF} = 1\text{kW}$. We see that the thresholds in a uniform plasma and pump electric field are low when compared with the experimental values (up to 100kW).

II-B. NUMERICAL RESULTS

We solved Eq. (1) numerically for ω_R/ω_0 and γ/ω_0, with χ_e and χ_i defined by Eqs. (2) and (3) respectively. In a given numerical search, we vary $k_\perp$ while specific values of n_e, T_e, L_n, B_T, P_{RF}, $k_{0||}$ and $k_{||}$ were kept constant (T_i was usually set equal to T_e). We calculate $E_{0||}$ and $E_{0\perp}$ from P_{RF} (net RF power injected by the waveguide array) using the WKB method [10]:

$$E_{0||}(x) = \frac{E_{0||WG}}{2^{1/2}}\left[\frac{\left(\frac{\omega_{pe}^2(x_{WG})}{\omega_0^2} - 1\right)\left(1 + \frac{\omega_{pe}^2(x_{WG})}{\omega_{ce}^2} - \frac{\omega_{pi}^2(x_{WG})}{\omega_0^2}\right)}{\left(\frac{\omega_{pe}^2(x)}{\omega_0^2} - 1\right)\left(1 + \frac{\omega_{pe}^2(x)}{\omega_{ce}^2} - \frac{\omega_{pi}^2(x)}{\omega_0^2}\right)}\right]^{\frac{1}{4}} \tag{17}$$

$$E_{0\perp}(x) = \frac{|k_{0\perp}(x)|}{|k_{0||}|}E_{0||}(x)$$

where $E_{0||WG}$ is the parallel component of the electric field at the waveguide mouth. In our slab model $E_{0\perp} = E_{0x}$ and $E_{0y} = 0$. $E_{0||WG}$ is calculated from the applied

RF power by requiring the conservation of power flux across the waveguide-plasma interface.

$$P_{RF} = [W_T v_{0x}]_{WG} L_y L_z \tag{18}$$

where $W_T = (E_0^2/16\pi)\omega_0(\partial\epsilon/\partial\omega_0)$ is the total wave energy density, v_{0x} is the group velocity in the x-direction and $L_y L_z$ is the total area of the waveguide array. The factor $1/2^{1/2}$ in Eq. (17) is included to account for power divided equally in two resonance cones (Fig. 1region B). In region A this factor should be omitted. We note that $E_{0\|}$ decreases and E_{0x} increases as the wave propagates radially inward to a region of higher plasma density. WKB approximation is not valid where $k_{0x}^{-1}(dk_{0x}/dx) \gtrsim k_{0x}$. For $k_{0\|} = 1\text{cm}^{-1}$, $L_n = 0.2\text{cm}$ (a typical experimental value in Alcator A), this is within 0.4cm of the critical layer $x = x_1$ $(\omega_{pe}/\omega_0 \lesssim 3)$. Since this is only a very narrow region near $\omega_{pe} = \omega_0$ where other effects may become important, in the present paper we have avoided this region. In addition, in most experiments the plasma is overdense at the waveguide mouth so as to optimize coupling.[11]

In Fig. 4(a) we show a typical result of our numerical calculation. The parameters used are: $n_e = 4 \times 10^{11}\text{cm}^{-3}$, $n_{WG} = 1.5 \times 10^{11}\text{cm}^{-3}$, $T_e = T_i =$ 3eV, $B = 5\text{T}$ ($B = 5\text{T}$ at the outer edge corresponds to $B = 6\text{T}$ at the plasma center), $f_0 = 2.45\text{GHz}$, deuterium plasma, $n_{0\|} = 2$, $n_{\|}^{-} = 5$ and $P_{RF} = 10\text{kW}$, which represent typical experimental conditions during the Alcator A lower hybrid heating experiments. ω_R/ω_0 and γ/ω_0 are plotted against $k\lambda_{De}$. Here, ω_R, γ and k are the real part of frequency, the growth rate and the magnitude of wavenumber of the quasi-mode, respectively. We note that the wavenumbers satisfy the usual selection rule $\mathbf{k} = \mathbf{k}_0 + \mathbf{k}^{-}$. A plot of γ/ω_0 vs. ω_R/ω_0 is shown in Fig. 4(b). We see that for $P_{RF} = 10\text{kW}$ the growth rates are comparable with the frequencies of the quasi-modes and that γ is maximum for $\omega_R/\omega_0 \simeq 10^{-3}$. In Alcator A where $f_0 = 2.45$GHz, this would predict $f \simeq 2.5$MHz for the most unstable quasi-mode at the particular density of $n_e = 4 \times 10^{11}\text{cm}^{-3}$ near the edge. We also note that the frequency width of this quasi-mode is of the order of the frequency at maximum growth rate. We find the results are quite insensitive to the relative orientation of $\mathbf{k}_{0\perp}$ and $\mathbf{k}_\perp^-$. Hence, we took $\mathbf{k}_{0\perp} \perp \mathbf{k}_\perp^-$ in all of our calculations. We also remark that if we used μ^- instead of μ, the difference in the maximum growth rate would be typically of the order of 10%.

Figure 5(a) shows the radial variation of ω_R/ω_0 and γ/ω_0 (where $\omega_R \equiv \omega_{Rmax}$ is the value of ω_R at maximum growth rate and $\gamma \equiv \gamma_{max}$) for the case of Alcator A with $a = 10$cm, $n_{0\parallel} = 2$, $n_\parallel^- = 5$, $P_{RF} = 10$kW, deuterium plasma and $B = 5$T ($B = 6$T at the plasma center). The assumed temperature and density profiles are shown in the inset. The density at the waveguide mouth was assumed to be $1.5 \times 10^{11}\text{cm}^{-3}$. The waveguide used in Alcator A had a flat interface vertically with the plasma at r=12.5cm (so the top and the bottom of the waveguide mouth were actually located behind the vacuum vessel wall). Although WKB theory is not strictly valid in the shaded region of Fig. 5(a), for the sake of comparison we have included results from this region. We do not expect the electric fields based on WKB calculations to differ appreciably from the actual electric fields near the waveguide mouth. We note that the growth rate is large at the edge ($\gamma/\omega_R \simeq 2$ at $r > 12$cm for $P_{RF} = 10$kW) and decreases significantly as the waves propagate inward. The dotted lines show solutions with the $\mathbf{E} \times \mathbf{B}$ coupling term neglected while the solid lines give the results when both the $\mathbf{E} \times \mathbf{B}$ and the $E_\parallel$ terms are retained. In agreement with Eq. (12), the $\mathbf{E} \times \mathbf{B}$ coupling term starts to dominate for $n_e \gtrsim 10^{13}\text{cm}^{-3}$. Figure 5(b) shows the variation of ω_R/ω_0 and γ/ω_0 as we vary $k_\parallel$ of the quasi-mode for the same conditions as Fig. 5(a) and $n_e = 4 \times 10^{11}\text{cm}^{-3}$,

$T_e = T_i = 3$eV. The parallel wavenumber of the lower sideband, $k_{\|}^{-}$, also increases as $k_{\|}$ is increased since $k_{0\|}$ is kept constant and $k_{\|}^{-} = k_{\|} - k_{0\|}$. For higher $k_{\|}$, ω_R ($\simeq k_{\|} v_{ti}$) is larger and so is the value of γ/ω_0. We note that lower hybrid waves having large values of $k_{\|}^{-}$ will be strongly electron Landau damped shortly beyond the plasma edge and will not propagate to the center of the plasma column. In Fig. 5(c) we show the power dependences of ω_R/ω_0 and γ/ω_0 for the same conditions as Fig. 5(b) and for $n_{\|}^{-} = 5$. The homogeneous (collisional) threshold for this case is less than 10W, and near the threshold we find $\omega_R \simeq 1.2 k_{\|} v_{ti}$.

Figures 6(a)–6(c) show similar results for Alcator C where a 4.6GHz RF system is used. The waveguide array consists of four rows and four columns and the width of one row of waveguides is 3.8cm and the height is 5.75cm.[12] The limiter radius for usual operations is $a = 16.5$cm. For this case we used the measured density and temperature at the waveguide mouth ($r = 17.8$cm or $r/a = 1.08$), namely $n_e \simeq 5 \times 10^{12}\text{cm}^{-3}$ and $T_e \simeq T_i \simeq 5$eV, respectively. Figure 6(a) shows the frequencies and the growth rates at various minor radii for $n_{0\|} = 3$, $n_{\|}^{-} = 5$, $P_{RF} = 40$kW, hydrogen plasma and $B = 8$T ($B = 10$T at the plasma center). We again note the large growth rates for $r/a \gtrsim 1.08$ (behind the waveguide mouth). Figure 6(b) shows the frequencies and the growth rates for different parallel wavenumbers of the quasi-mode for the same conditions as Fig. 6(a) and for $n_e = 5 \times 10^{12}\text{cm}^{-3}$ and $T_e = T_i = 5$eV. Figure 6(c) shows the frequencies and the growth rates vs. applied RF power for the same conditions as Fig. 6(b) and $n_{\|}^{-} = 5$. The homogeneous threshold for this case at $r = 17.8$cm is $P \lesssim 4$kW.

III. CONVECTIVE THRESHOLD

Here we shall examine the thresholds due to the finite length of the wave launcher and the finite width of the resonance cones.[10] We shall take L_z as the extent of the coupler along the toroidal direction, and L_y as that in the poloidal direction. For simplicity we shall assume here that the plasma is spatially homogeneous. In this section we shall consider only accessible waves ($n_{0\|} > n_{\|ac}$), and for simplicity we shall assume $E_{0y} = 0$.

III-A. $E_\|$ COUPLING

For this case, the decay lower hybrid wave can propagate almost parallel to the pump wave. The decay wave is assumed to propagate in the x-z plane to minimize the convective loss. The homogeneous convective threshold can be estimated by[13-15]

$$\frac{\gamma \Delta x}{|v_{2x}|} = \frac{\gamma L_z}{\left| v_{2x}\left(\dfrac{v_{2z}}{v_{2x}} - \dfrac{v_{0z}}{v_{0x}}\right)\right|} = \pi \tag{19}$$

where γ is the homogeneous growth rate and $\Delta x \equiv L_z/|v_{2z}/v_{2x} - v_{0z}/v_{0x}|$ is the maximum distance the decay wave can travel in the x-direction before it convects out of the pump resonance cone (see Fig. 7). In order to get this threshold, an $\exp(2\pi)$ growth of the decay wave power was assumed. If the power level of the background lower hybrid waves were already enhanced by the presence of the pump lower hybrid wave due to scattering from previously existing low frequency density fluctuations, Eq. (19) may give an overestimate of the convective threshold.

The convective threshold is determined as follows: we first obtain the homogeneous plasma growth rate needed for this threshold γ_{th} from Eq. (19). We can then obtain the threshold RF power from a graph of γ/ω_0 vs. P_{RF} such as shown in Figs. 5(c) and 6(c). However, we can get a rough analytic estimate of this threshold using either Eq. (13) or Eq. (15) depending on the power level relative to the threshold power.

At the edge, $\omega_2 \simeq \omega_{pe}(k_{2z}/k_2)$, so $v_{2z} \equiv \partial\omega_2/\partial k_{2z} = (\omega_2/k_{2z})(k_{2x}^2/k_2^2)$, $v_{2x} \equiv \partial\omega_2/\partial k_{2x} = -(\omega_2/k_{2x})(k_{2x}^2/k_2^2)$, where we took $k_{2\perp} = k_{2x}$, $k_{2y} = 0$. The threshold given by Eq. (19) can then be estimated as

$$E_{0\parallel}^2 \simeq \frac{4}{F}\frac{m_e^2\omega_0^2}{e^2}\frac{T_i}{m_e}\left[\frac{\nu_e}{\omega_0} + \left(\frac{k_{2x}}{k_2}\right)^3 \frac{2\pi}{k_{2z}L_z}\frac{\omega_0 - \omega_2}{\omega_0}\right] \tag{20}$$

where we have used Eq. (13) since $\gamma_{th}/\omega_0 < k_\parallel v_{ti}/\omega_0$ and we have kept the collisional threshold term. The second term in the bracket can be of the order of ν_e/ω_0 or less, in which case the threshold is essentially the same as the collisional threshold. However, to obtain this low threshold Δx, the distance the parametrically excited lower hybrid wave has to travel in the x-direction, may become larger than the plasma minor radius and Eq. (20) is no longer valid. Furthermore, effects of density and temperature gradients must be considered, including large variations in γ due to the changing plasma parameters. These problems will be examined in Sec. IV.

III-B. $E \times B$ COUPLING

For this case the decay wave has to travel at an angle with respect to the pump resonance cone (see Fig. 8) since coupling tends to vanish as k_{2y} approaches zero. In general, if k_{2y}/k_{2x} is large, the $\mathbf{E} \times \mathbf{B}$ driving term is large (Eq. (5)) but the convective loss is also large. On the other hand, if k_{2y}/k_{2x} is small, the convective loss is small but the $\mathbf{E} \times \mathbf{B}$ driving term also becomes small. The optimum angle of propagation for the decay lower hybrid wave can be found by maximizing $\gamma\Delta x/|v_{2x}|$ with respect to the angle ϕ that $\mathbf{k}_{2\perp}$ makes with the x-direction.[15] For the $\mathbf{E} \times \mathbf{B}$ dominated decay γ is proportional to $k_{2y}^{2/3}$ well above threshold,

$v_{2x} = -(k_{2x}\omega_2/k_2^2)(1 - \omega_{LH}^2/\omega_2^2)$, $v_{2z} = (\omega_2/k_{2z})(1 - \omega_{LH}^2/\omega_2^2)$, and we find $\cos\phi = -A + (A^2 + 3)^{1/2} \simeq 1 - (1/2)(\omega/\omega_0)$ for optimum convective growth in the x-z plane, where $A \equiv (k_2^2/k_{2z}k_{2\perp})(k_{0z}k_{0\perp}/k_0^2) \simeq 1 + (\omega/\omega_0)$ for $\omega/\omega_0 \ll 1$ and for $\omega_{LH}^2 \ll \omega_0^2$. Convective growth in the y-direction is also optimized for $k_{2y} \ll k_{2x}$ since γ increases only like $k_{2y}^{2/3}$ but $|v_{2y}|$ increases like k_{2y}. We get $k_{2y} \ll k_{2x}$ ($\cos\phi = 0.9995$ for $\omega/\omega_0 = 10^{-3}$) and we can use Eq. (19) to calculate the convective threshold for this case. However, we note that the coupling is lost and the growth rate is reduced by the factor $(1 - \cos^2\phi)^{1/3} \simeq (\omega/\omega_0)^{1/3} \simeq 10^{-1}$ from the optimum coupling case $k_{2y} = k_{2\perp}$ in order to get the low convective loss (which corresponds to a factor of 1000 in RF power). In addition, there remains the same problem that Δx is large.

Here we shall consider the case when the $\mathbf{E} \times \mathbf{B}$ driving term is maximized so that $k_{2y} = k_{2\perp}$ and $k_{2x} = 0$. Then the convective thresholds in the y- and z-directions, respectively, are:

$$\frac{\gamma L_y}{|v_{2y}|} \simeq \frac{\gamma L_y |k_{2y}|}{\omega_2\left(1 - \dfrac{\omega_{LH}^2}{\omega_0^2}\right)} = \pi$$

$$\frac{\gamma L_z}{|v_{2z}|} \simeq \frac{\gamma L_z |k_{2z}|}{\omega_2\left(1 - \dfrac{\omega_{LH}^2}{\omega_0^2}\right)} = \pi$$

where we have used $|k_{2y}| \simeq k_2$, which is valid in the $\mathbf{E} \times \mathbf{B}$ coupling regime. There is no convective loss in the x-direction because we have assumed that $k_{2x} = 0$. Convective loss in the z-direction dominates because $L_z < L_y$ and $|k_{2z}| < |k_{2y}| \simeq |k_{2\perp}|$ for the present case.

Since we find that $\gamma_{th}/\omega_0 \gg k_{\parallel}v_{ti}/\omega_0$, we have to use Eq. (16) for the homogeneous growth rate and we get

$$E_{0x}^2 \simeq \frac{10}{3^{1/2}} \frac{B^2}{c^2} \left(\frac{k^-}{k_y^-} \right)^2 \frac{\omega_0^2}{\omega_{LH}^2} \frac{\omega_0^2}{k_z^2} \left(\frac{\pi}{|k_{2z}| L_z} \right)^3$$

as the estimate for this threshold. More precisely, one should use the numerical growth rate as in the previous sub-section. For the Alcator A edge conditions and for $n_{2\|} = 5$ we get $\gamma_{th}/\omega_0 \simeq 0.5$, a value that can never be achieved and therefore the $\mathbf{E} \times \mathbf{B}$ coupling in the outer plasma layers is not expected to play a significant role under the assumed conditions.

IV. THRESHOLD DUE TO FINITE RADIAL GROWTH REGION

IV-A. CASE WITH WELL-DEFINED RESONANCE CONES

In this case we consider a pump wave packet characterized by $n_{0\|} > n_{\|ac}$, such that the pump wave penetrates into the plasma but is confined between resonance cones.[10] Initially these waves have $\mathrm{v}_{0\perp}$ oriented mainly along the x-direction. As shown in Section II–B, the homogeneous growth rate associated with the $E_{\|}$ coupling is strongly peaked near the edge. Furthermore, we have seen that the convective threshold for this decay process is very high if the coupling is dominated by the $\mathbf{E} \times \mathbf{B}$ term. Therefore, the lowest threshold will be associated with $E_{\|}$ coupling, but only if the radial (*i.e.*, x-direction) growth distance Δx is small compared to the plasma radius a (*i.e.*, $\Delta x \ll a$).

To optimize the large growth rates due to $E_{\|}$ near the plasma periphery, we shall consider a factor of $\exp(2\pi)$ growth in the decay wave power within a distance L_x ($L_x \ll a$) from the waveguide mouth (Fig. 1).

$$\int \frac{2\gamma(x)}{|v_{2x}(x)|}\, dx = 2\pi$$

where the range of integration is from the waveguide mouth to the plasma center. This can be estimated roughly by

$$\frac{\gamma L_x}{|v_{2x}|} = \left[\frac{\gamma}{\omega_2}\left(\frac{k_2}{k_{2x}}\right)^2 |k_{2x}| L_x\right]_{x=x_{WG}} = \pi \tag{21}$$

where L_x is the effective growth distance in the radial direction. This condition can give a relatively low threshold only if $|k_{2x}| < |k_{2y}| \simeq |k_{2\perp}|$.

The convective threshold in the y-direction for the present case is

$$\frac{\gamma L_y}{|v_{2y}|} \simeq \frac{\gamma}{\omega_2}\left(\frac{k_2}{k_{2y}}\right)^2 |k_{2y}| L_y = \pi, \tag{22}$$

whereas that in the x-z plane given by Eq. (19) can be rewritten as

$$\frac{\gamma}{\omega_2}\left(\frac{k_2}{k_{2x}}\right)^2 \frac{|k_{2x}|L_z}{\left|\dfrac{k_2^2}{k_{2z}k_{2x}} - \dfrac{k_0^2}{k_{0z}k_{0x}}\right|} = \pi, \tag{23}$$

where $\omega_{LH}^2 \ll \omega_0^2$ is assumed. The highest of the thresholds given by Eqs. (21), (22) and (23) determines the threshold. Note that the threshold (21) can be made smaller than the threshold (22) for

$$\left|\frac{k_{2x}}{k_{2y}}\right| < \frac{L_x}{L_y} \ll 1. \tag{24}$$

If this is true, the threshold Eq. (21) reduces to

$$\frac{\gamma L_z}{|v_{2z}|} = \pi$$

which is just the convective threshold in the z-direction. The convective threshold in the z-direction is always higher than that in the y-direction under the assumed conditions since $(L_y/L_z)(\omega_{pe}/\omega_0) > 1$. But the convective threshold in the z-direction may not exist in the standing wave region A of Fig. 1.

We now consider the decay occurring in the region A and take Eq. (22) to be the relevant threshold. We take the situation shown in Fig. 9, *i.e.*, $k_{0x} \simeq k_{1x} \gg k_{2x}$, $k_{1y} \simeq -k_{2y} \gg k_{0y}$ so that Eq. (24) is satisfied. In this case the threshold becomes

$$\begin{aligned}\frac{\gamma_{th}}{\omega_0} &= \frac{\pi}{|k_{2z}|L_y}\left|\frac{k_{2y}}{k_2}\frac{k_{2z}}{k_2}\right| \\ &\simeq \frac{c}{2f_0|n_{2\|}|L_y}\frac{\omega_0}{\omega_{pe}}.\end{aligned} \tag{25}$$

Table I shows some examples of threshold (25). Since $c/(2f_0 n_{2\|}L_y) \simeq 0.1$ for Alcator A and for $n_{2\|} \simeq 5$, this threshold is very high unless $\omega_{pe} \gg \omega_0$ or $n_{2\|} \gg 5$.

We see that in Alcator A, this threshold is not reached even with $P_{RF} = 1\text{MW}$ for $n_{\parallel}^{-} = 5$. Even for $n_{\parallel}^{-} = 20$ this threshold is greater than the available power of 100kW. Furthermore, these waves will be Landau damped in the edge region with $T_e \simeq 100\text{eV}$ and never propagate to the center.

IV–B. CASE WITH UNIFORM PUMP WAVE SHELL

In the Alcator A experiment a two-waveguide array was used as an antenna.[1] In such a geometry a significant fraction of the total RF power is contained in the inaccessible part of the $n_{0\parallel}$ spectrum, namely $1 \leq n_{0\parallel} \leq n_{\parallel ac}$. These components of the pump electric field will be confined to the outer plasma region which extends from the slow wave cut-off layer ($\omega = \omega_{pe}$) to the slow wave-whistler wave mode conversion layer[16]

$$\frac{\omega_{pi}}{\omega_0} = n_{0\parallel} y \mp [1 + n_{0\parallel}^2 (y^2 - 1)]^{1/2} \tag{26}$$

where $y \equiv \omega_0/(\omega_{ce}\omega_{ci})^1/2$. Due to toroidal effects[5] the pump wave acquires large values of the poloidal wavenumber such that $k_{0y} \gg k_{0x}$, and then the wave will propagate mostly in the poloidal-toroidal plane. The combined effects of magnetic shear and rotational transform may increase $n_{0\parallel}$ to values larger than $n_{\parallel ac}$, and the pump wave will penetrate to the plasma interior. In this process we expect that a shell of outer pump wave region with a thickness δr and circumference $2\pi a$ (*i.e.*, a volume $(2\pi R)(2\pi a)\delta r$ where a and R are the minor and major radii of the tokamak plasma) will be formed. In a real tokamak, this pump wave shell is deformed due to the $1/R$ dependence of the toroidal field so that the width of the shell is narrower on the outside of the torus. For simplicity, we shall neglect this effect and we shall assume that this region is filled uniformly with the pump wave.

To examine this model in more detail, let us consider the dispersion relationship near the plasma surface. The fourth-order equation for $n_\perp$ can be split in two roots,[16,17] namely the slow wave

$$\begin{aligned} n_\perp^2 &= \frac{P}{S}(S - n_\parallel^2) \\ &\simeq \left(\frac{\omega_{pe}^2}{\omega^2} - 1\right)(n_\parallel^2 - 1), \end{aligned} \tag{27}$$

and the fast wave

$$\begin{aligned} n_\perp^2 &= (S - n_\parallel^2) - \frac{D^2}{(S - n_\parallel^2)} \\ &\simeq \frac{\omega_{pe}^4}{\omega^2 \omega_{ce}^2} \frac{1}{(n_\parallel^2 - 1)} - (n_\parallel^2 - 1). \end{aligned} \tag{28}$$

Here $P = 1 - \omega_{pe}^2/\omega^2 - \omega_{pi}^2/\omega^2 \simeq -\omega_{pe}^2/\omega^2$, $S = 1 + \omega_{pe}^2/\omega_{ce}^2 - \omega_{pi}^2/\omega^2 \simeq 1$ and $D \simeq \omega_{pe}^2/(\omega\omega_{ce})$. In obtaining Eqs. (27) and (28), we assumed that $\omega_{ci}^2 \ll \omega^2 \ll \omega_{pe}^2 \ll \omega_{ce}^2$, and that the waves are not near the mode conversion layer given by Eq. (26). The region δr is confined between the critical densities given by Eq. (27) (taking $n_\perp^2 = 0$, *i.e.*, $\omega_{pe}^2 = \omega^2$) and Eq. (26) (take the negative sign for the first mode conversion layer), and its value is typically a small fraction of the plasma minor radius. Note that the fast wave (whistler) cut-off layer is between the critical densities found from Eqs. (26) and (27), and thus it is also contained within δr.

In the limit $\omega_{pe}^2 \gg \omega^2$, the group velocity of the slow wave is deduced from Eq. (27) as

$$\begin{aligned} v_\parallel &\equiv \frac{\partial\omega}{\partial k_\parallel} = \frac{c}{n_\parallel} \\ v_\perp &\equiv \frac{\partial\omega}{\partial k_\perp} = -v_\parallel \frac{\omega}{\omega_{pe}}\left(1 - \frac{1}{n_\parallel^2}\right)^{1/2} \end{aligned}$$

and that of the fast wave follows from Eq. (28):

$$v_{\parallel} = cn_{\parallel}\frac{D^2+(n_{\parallel}^2-1)^2}{n_{\parallel}^2D^2+(n_{\parallel}^2-1)^2}$$

$$v_{\perp} = c(n_{\parallel}^2-1)^{3/2}\frac{[D^2-(n_{\parallel}^2-1)^2]^{1/2}}{n_{\parallel}^2D^2+(n_{\parallel}^2-1)^2}.$$

We note that waves having different values of $n_{\parallel}$ propagate at different angles to each other and as a consequence they tend to diverge instead of propagating inside a resonance cone as the density varies. Toroidal effects and scattering from turbulent density fluctuations will further accentuate this phenomenon. Here we shall consider the case when the pump lower hybrid wave has uniformly filled the outer pump wave shell. If, in addition, the parametrically excited lower hybrid waves propagate mainly in the y-z plane, (*i.e.*, the poloidal-toroidal plane) we recover the case of the homogeneous threshold of Sec. II–A. The decay waves will keep amplifying until due to the small but finite k_x they get out of the region filled with the pump wave. We note that in order to explain the enhanced low-frequency fluctuations observed on the probe located in the shadow of the limiter by this mechanism, the decay had to occur at the location of the probe. If the decay occurred only in front of the waveguide, the quasi-mode would damp as soon as it would leave the growth region and a probe at a different location would not detect the enhanced low-frequency fluctuations.

The threshold electric field for this case is given by Eq. (14) but it is not so easy to calculate this field from the RF power at the waveguide. We can estimate the RF threshold power as follows: assume that ξ is the fraction of RF power in the inaccessible region of $n_{0\parallel}$, and that this power fills uniformly the cylindrical volume $(2\pi a\delta r)(2\pi R)$. Applying conservation of power flux across a cross sectional surface of this cylindrical volume at one poloidal plane, we get

$$Q\xi P_{RF} = W_T v_{0\parallel} 2\pi a(\delta r)$$

where W_T is defined in Eq. (18). The quantity Q is the enhancement factor due to the fact that the pump wave may propagate around the torus several times before it loses its energy by collisions. We define $Q \equiv (1 - P_1/P_0)^{-1}$ where $P_1/P_0 \equiv \exp(-2\pi R\nu_e/v_{0\|})$ is the fraction of the pump wave power left after one toroidal pass. Now since $\partial\epsilon/\partial\omega_0 \simeq 2/\omega_0$,

$$W_T \simeq \frac{E_{0\perp}^2}{8\pi} \simeq \frac{E_{0\|}^2}{8\pi}\left(\frac{k_{0\perp}}{k_{0\|}}\right)^2 \simeq \frac{E_{0\|}^2}{8\pi}\frac{\omega_{pe}^2}{\omega_0^2}.$$

Hence, the threshold electric field is given by

$$P_{RF} \simeq \frac{E_{0\|}^2}{8\pi}\frac{\omega_{pe}^2}{\omega_0^2}\frac{c}{n_{0\|}}\frac{2\pi a(\delta r)}{\xi Q}.$$

For Alcator A, $Q \simeq 14$, $\xi \simeq 0.4$, $a = 10$cm, $\delta r \simeq 2$cm, and taking $\omega_{pe}^2/\omega_0^2 \simeq 5$, for the threshold we get $P_{RF} \simeq 90$W for $E_{0\|} = 0.03$kV/cm which should be compared with the $P_{RF} \simeq 80$kW injected power. For Alcator C we take $Q \simeq 3$, $\xi \simeq 0.2$, $a = 16.5$cm, $\delta r \simeq 3$cm, and for $\omega_{pe}^2/\omega_0^2 \simeq 5$ we get $P_{RF} \simeq 4$kW for $E_{0\|} = 0.04$kV/cm (homogeneous threshold electric field for $\omega_{pe}^2/\omega_0^2 \simeq 5$ and $T_e = T_i = 3$eV). Again, the $P_{RF} \simeq 650$kW power injected into this device can exceed this threshold. We note that the convective threshold for the $\mathbf{E} \times \mathbf{B}$ driven decay (such as the ion-cyclotron quasi-mode decay) can also be significantly reduced inside this pump wave shell.

Concluding this section we remark that applying these calculated thresholds to actual experiments assumes a pump wave with a narrow bandwidth. If the surface of the plasma is turbulent, and the pump wave frequency spectrum broadens sufficiently due to this turbulence such that $\Delta\omega/\omega_0 \simeq \gamma/\omega_0$, then there is some question in applying these thresholds.[18-20] In this paper we shall not calculate the effects of such low frequency density fluctuations.

V. THRESHOLDS DUE TO DENSITY GRADIENTS AND TEMPERATURE GRADIENTS

In the parametric decay process under consideration the following selection rules must be satisfied:

$$\omega_2 = \omega_0 - \omega \tag{29}$$

$$\mathbf{k}_2 = \mathbf{k}_0 - \mathbf{k} \tag{30}$$

where

$$\omega \simeq k_{\|} v_{ti} \tag{31}$$

$$\omega_2 \simeq \omega_{pe} \frac{k_{2\|}}{k_2}; \qquad \omega_0 \simeq \omega_{pe} \frac{k_{0\|}}{k_0}. \tag{32}$$

Let us first consider the case of inhomogeneous density, but spatially uniform temperatures. For a given T_i and $k_{\|}$, ω is fixed through Eq. (31). Equation (29) can be satisfied with the same value of ω_2. As the waves propagate radially inward to a region of higher density, $\mathbf{k}_{0\perp}$ and $\mathbf{k}_{2\perp}$ change in order to satisfy the dispersion relationship Eq. (32). Since there is no restriction on $\mathbf{k}_{\perp}$, it can always be chosen so as to satisfy Eq. (30). Therefore, density gradients do not introduce new thresholds.

Let us now consider the case when both the density and temperature vary in the radial direction. In this case, ω changes as the waves propagate inward to a region of higher temperature. Equation (30) can still be satisfied as in the case of density gradients only, but Eq. (29) can no longer be satisfied with the same value of ω_2 and frequency mismatch occurs. But we have seen in Section II–B that the frequency spectrum of the quasi-mode is quite broad (except at powers very close to threshold) and $\Delta\omega_H$ is typically of the order of ω_R. Therefore, the effect of mismatch is not so important unless $L_x \gtrsim L_T$ where $L_T \equiv T|dT/dx|^{-1}$ and L_x was defined in Sec. IV-A. Thus we shall take $L_x \ll L_T$ and the thresholds obtained in Sec. III–B remain valid. We also remark that the effect of gradients does not play an important role for the case considered in Sec. IV–B where parametric decay occurs mainly in the outer plasma shell.

VI. PUMP DEPLETION

If the decay waves remain small in amplitude, the pump wave power can be considered as essentially constant along its trajectory. However, if the decay waves are amplified to such an extent that significant fraction of the pump power is transferred to the decay waves, the power contained in the pump wave decays as it propagates towards the plasma center.

The spatial evolution of the pump and the sideband powers after reaching a steady state is described by the following coupled equations[21,22]

$$\begin{aligned} \mathrm{v}_0 \cdot \nabla I_0 &= -\alpha I_0 I_2 \\ \mathrm{v}_2 \cdot \nabla I_2 &= +\alpha I_0 I_2 \end{aligned} \tag{33}$$

where $I_0(x,y,z) \equiv E_0^2(x,y,z)/\omega_0$ and $I_2(x,y,z) \equiv E_2^2(x,y,z)/\omega_2$ are the action variables, v_0 and v_2 are the group velocities of the pump wave and the sideband lower hybrid wave, respectively, and

$$\begin{aligned} \alpha &\equiv \frac{\mu^2}{4} \frac{\omega_0^2}{E_{0WG}^2} \left(1 + \frac{\omega_{pe}^2}{\omega_{ce}^2}\right)^{-1} \mathrm{Im}\left(\frac{\chi_e \chi_i}{\epsilon}\right) \\ &= \frac{2\gamma\omega_0}{E_{0WG}^2}. \end{aligned}$$

Here E_{0WG} is the pump electric field at the waveguide mouth, Im is the imaginary part, and γ is the linear growth rate. It can be seen from Eq. (33) that $\nabla \cdot (\mathrm{v}_0 I_0 + \mathrm{v}_2 I_2) = 0$ and the action flux is conserved. In the limit $\omega \ll \omega_2 \simeq \omega_0$, the power flux is conserved among the pump wave ω_0 and the lower sideband ω_2 (there is negligible power going into the low frequency mode ω).

Here, we consider the case when a uniformly filled pump wave shell exists in the outer layers of the plasma (the case discussed in Sec. IV–B). Significant pump depletion is not expected when well-defined resonance cone exists since the convective threshold for this case was found to be high in Sec. IV–A. This case is reviewed in the Appendix. Since the pump wave is assumed to fill the outer shell region of the plasma, there are no convective losses in the y- and z-directions and Eq. (33) reduces to

$$\frac{\partial G_0}{\partial x} = -G_0 G_2$$
$$\frac{\partial G_2}{\partial x} = +G_0 G_2$$

where $G_0 \equiv \alpha I_0/v_{2x}$, $G_2 \equiv \alpha I_2/v_{0x}$. The pump wave is now assumed to be homogeneous in the shell region of thickness L_x so the boundary conditions become

$$G_0 = A_0$$

$$G_2 = A_2$$

at $x = 0$. Solving for G_0 and G_2 within the shell region gives

$$G_0 = \frac{A_0}{\dfrac{A_0}{A_t} + \dfrac{A_2}{A_t}\exp(A_t x)},$$
$$G_2 = \frac{A_2 \exp(A_t x)}{\dfrac{A_0}{A_t} + \dfrac{A_2}{A_t}\exp(A_t x)}$$

where $A_t \equiv A_0 + A_2$. Half of the pump wave power will be depleted within the x-distance L_x if

$$A_t L_x = \frac{2\gamma L_x}{|v_{2x}|} > \ln\left(\frac{A_0}{A_2}\right)$$

so that appreciable pump depletion is not expected unless $|v_{2x}| \ll |v_{2y}|$, *i.e.*, when the decay wave propagates mainly in the y-direction (and therefore, can spend a long time inside the pump wave shell).

In reality, the situation is more complex. The pump wave fills up the shell region by undergoing many reflections from the lower hybrid–whistler wave mode conversion layer and the plasma wave cut-off layer and the location of the mode conversion layer is different for different $n_{\|}$'s. Moreover, the source of the pump wave is localized both toroidally and poloidally. However, the analysis given in the present section remains valid in an approximate sense.

VII. SUMMARY AND CONCLUSIONS

The results of analytic and numerical calculations of the growth rates and various thresholds for parametric decay of a lower hybrid pump wave into another lower hybrid wave and a low frequency ion-sound quasi-mode were presented. It was found that for the Alcator A edge plasma parameters, the frequency of this quasi-mode is of the order of a few MHz ($\omega_R/\omega_0 \simeq 10^{-3}$) and the homogeneous growth rate at the edge region is large ($\gamma/\omega_R \gtrsim 1$) even for modest pump powers. The growth rate for this instability is found to follow the well-known $\gamma + \Gamma_2 \sim E_0^2$ scaling for quasi-mode decay for low pump powers such that $\gamma \ll \omega_R$. However, at larger pump powers such that $\gamma \gtrsim \omega_R$, the growth rate increases only like $\gamma \sim E_0^{2/3}$ (reactive quasi-mode).

Various inhomogeneous thresholds were estimated, including an $\exp(2\pi)$ growth within a small radial distance L_x from the plasma edge. If we assume an accessible, well-defined pump resonance cone, the convective threshold for $\exp(2\pi)$ growth becomes very large ($P >$ 1MW for $n_{\parallel}^{-} = 5$). But if we assume that the pump wave stays on the outer layer of the plasma, as is expected for pump waves in the inaccessible range of $n_{0\parallel}$ spectrum, the convective thresholds are greatly reduced and we can get a low threshold as discussed in Sec. IV–B.

The efficiency of pump depletion has been estimated. Typically, the pump depletion becomes effective when the pump power exceeds a few times the $\exp(2\pi)$ convective threshold and the power in the decay waves exceeds that in the pump wave. For the accessible part of the $n_{\parallel}$ spectrum, this power is very high. But the inaccessible waves that stay on the outer surface of the plasma may get depleted.

This process could explain the results from the Alcator A lower hybrid heating experiments, namely: (i) frequency downshifted and frequency broadened RF spectrum and enhanced low-frequency fluctuations; (ii) ion tail formation which was found to be independent of the phasing of a two-waveguide grill. Of course, below the thresholds calculated in this paper we expect that scattering of the pump wave by the low frequency fluctuations would remain. However, above threshold the present process would dominate if the effect of pump frequency broadening due to such low frequency fluctuations can be neglected when compared with ω_R of the present decay process.

In Alcator C and in other lower hybrid heating experiments,[23-26] the pump $n_{0\|}$ spectrum is better defined and there is less fractional power in the inaccessible part of $n_{0\|}$ spectrum than in Alcator A. Therefore, this process may be less important in these devices. However, during current drive experiments lower $n_{0\|}$ components increase again and the present parametric process may become important again at high densities.

VIII. ACKNOWLEDGMENT

The authors wish to acknowledge valuable discussions with Dr. J. J. Schuss. This work was supported by the U.S. Department of Energy, Contract No. DE-AC02-78ET51013.

APPENDIX: PUMP DEPLETION FOR THE CASE WITH WELL-DEFINED RESONANCE CONE

First, consider the case when $v_{2y} = 0$ (*i.e.*, $k_{2y} = 0$). The geometry is shown in Fig. 7. The pump wave is also assumed to propagate in the x-z plane so that $v_{0y} = 0$. In this case Eq. (33) can be written in a two-dimensional form

$$\begin{aligned} \frac{\partial G_0}{\partial x} + C_0 \frac{\partial G_0}{\partial z} &= -G_0 G_2 \\ \frac{\partial G_2}{\partial x} + C_2 \frac{\partial G_2}{\partial z} &= +G_0 G_2 \end{aligned} \tag{34}$$

where $C_0 \equiv v_{0z}/v_{0x}$, $C_2 \equiv v_{2z}/v_{2x}$ and $G_0 \equiv \alpha I_0/v_{2x}$, $G_2 \equiv \alpha I_2/v_{0x}$. G_0 and G_2 are proportional to the power flux in the radial direction of the pump wave and the decay wave, respectively.

The boundary condition for the case of uniform finite extent pump wave and a uniform initial noise level (which may be enhanced over the thermal noise) for the lower sideband can be written as

$$G_0 = \begin{cases} A_0 & \text{for} \quad -\dfrac{L_y}{2} < y < \dfrac{L_y}{2}, -\dfrac{L_z}{2} < z < \dfrac{L_z}{2} \\ 0 & \text{otherwise} \end{cases} \tag{35}$$

and $G_2 = A_2$ (everywhere) on the plane $x = 0$. The solutions of Eq. (34) with the boundary condition Eq. (35) in region A of Fig. 7 (*i.e.*, $|z - C_0 x| < L_z/2$, $|z - C_2 x| < L_z/2$, and $-(L_y/2) < y < (L_y/2)$) are given by[21,22]

$$G_0 = \frac{A_0}{\dfrac{A_0}{A_t} + \dfrac{A_2}{A_t}\exp(A_t x)} \tag{36}$$

$$G_2 = \frac{A_2 \exp(A_t x)}{\dfrac{A_0}{A_t} + \dfrac{A_2}{A_t}\exp(A_t x)} \tag{37}$$

and in region B (*i.e.*, $|z - C_0 x| < L_z/2$, $z - C_2 x < -L_z/2$, and $-(L_y/2) < y <$

$(L_y/2)$) by

$$G_0 = \frac{A_0}{\dfrac{A_0}{A_t} + \exp(A_2 x)\exp\left[A_0\left(\tau - \dfrac{L_z}{2V}\right)\right] - \dfrac{A_0}{A_t}\exp\left[A_t\left(\tau - \dfrac{L_z}{2V}\right)\right]}, \tag{38}$$

$$G_2 = \frac{A_2\exp(A_2 x)\exp\left[A_0\left(\tau - \dfrac{L_z}{2V}\right)\right]}{\dfrac{A_0}{A_t} + \exp(A_2 x)\exp\left[A_0\left(\tau - \dfrac{L_z}{2V}\right)\right] - \dfrac{A_0}{A_t}\exp\left[A_t\left(\tau - \dfrac{L_z}{2V}\right)\right]}. \tag{39}$$

Here, $V \equiv C_0 - C_2$ and $\tau \equiv -(z - C_0 x)/V$. It can be seen form Eq. (36) that the characteristic scale length for the decay wave growth in the x-direction is A_t^{-1}. This agrees with the result obtained in Sec. III–A since Eq. (36) also predicts an $\exp(2\pi)$ growth in the decay wave power at the point C in Fig. 7 for

$$A_t \Delta x = \frac{2\gamma \Delta x}{v_{2x}} \simeq 2\pi$$

where $A_2/A_0 \ll \exp(2\pi)$ is assumed and $\Delta x \equiv L_z/|V|$ is the same Δx defined in Sec. III–A. It is clear that half of the pump power will be depleted at point C in Fig. 7 when $A_t \Delta x = \ln(A_0/A_2)$ which is a few times above the $\exp(2\pi)$ convective threshold.

The fraction of the pump wave power that is depleted can be calculated in region B of Fig. 7 using the expression for G_0 given in Eq. (38)[21]:

$$\begin{aligned}\eta(x) &\equiv 1 - \int_{-\infty}^{\infty} \frac{dz}{L_z}\frac{G_0}{A_0} \\ &\simeq \frac{A_2}{A_0}\left[A_0\left(x + \frac{L_z}{2V}\right) + 1\right]\left[(e^\Gamma - 1)/\Gamma - 1\right]\end{aligned}$$

where $\Gamma \equiv A_t \Delta x$ is the spatial growth factor, and the assumptions $|A_2(x + L_z/2V)e^\Gamma| < 1$ and $|A_2 e^\Gamma/A_0| < 1$ were made in obtaining this result.

If $k_{2y} \neq 0$, the $v_{2y}(\partial I_2/\partial y)$ term in Eq. (33) must be retained. However, after performing the shear coordinate transformation:

$$x' = x$$

$$y' = y$$

$$z' = z - ax - by$$

where $a \equiv (v_{0z}v_{2y} - v_{0y}v_{2z})/(v_{0x}v_{2y} - v_{0y}v_{2x})$ and $b \equiv (v_{0x}v_{2z} - v_{0z}v_{2x})/(v_{0x}v_{2y} - v_{0y}v_{2x})$, the problem can be reduced to that in 2-dimensions. The transformed equations are:

$$\frac{\partial G_0}{\partial x'} + C_0 \frac{\partial G_0}{\partial y'} = -G_0 G_2$$
$$\frac{\partial G_2}{\partial x'} + C_2 \frac{\partial G_2}{\partial y'} = +G_0 G_2$$

where $C_0 \equiv v_{0y}/v_{0x}$, $C_2 \equiv v_{2y}/v_{2x}$. The transformed equations are independent of z' which is now a parameter that specifies a plane parallel to the plane that is spanned by the two vectors $\mathbf{v}_0$ and $\mathbf{v}_2$. On a given plane specified by z', this case reduces to the two dimensional case discussed above. For a finite extent uniform pump field given by Eq. (35), the transformed boundary condition on the plane $x' = 0$ becomes

$$G_0 = \begin{cases} A_0 & \text{for} \quad -\frac{L_y}{2} < y' < \frac{L_y}{2}, -\frac{L_z}{2} - z' < by' < \frac{L_z}{2} - z' \\ 0 & \text{otherwise} \end{cases}$$

and the background fluctuation level is again given by $G_2 = A_2$ (everywhere). The geometry, projected on the x-y plane, is shown in Fig. 8.

Consider the case when $k_{0y} = 0$, $|k_{2x}| \ll |k_{2y}|$, and take the plane $z' = 0$. In this case $|b| = |v_{2\parallel}/v_{2y}| = \omega_{pe}/\omega_2 > 1 > L_z/L_y$ so that the boundary condition for G_0 becomes $G_0 = A_0$ for $-L_z/2|b| < y' < L_z/2|b|$. G_0/A_0 and G_2/A_0 for the case $C_0 = 0$, $C_2 = 10$, $A_0(L_z/2|b|) = 150$ (corresponding to $\gamma/\omega_0 \simeq 2$ for

Alcator A and $n_{2\parallel} = 5$), and $A_2/A_0 = 10^{-4}$ are shown in Figs. 10(a) and 10(b) respectively. In this case the decay lower hybrid waves were assumed to travel in the $+y$-direction for simplicity, but there may also be waves traveling in the $-y$-direction. The fraction of the power remaining in the pump is plotted against the radial distance in Fig. 10(c). The pump does not get completely depleted in this case because of the assumption that the decay wave travels only in the $+y$-direction so that the depletion is not efficient near $y = -L_z/2|b|$. For usual values of γ/ω_0 ($\lesssim 10^{-2}$), no significant pump depletion is expected when the pump wave propagates inside a resonance cone.

IX. REFERENCES

[1]J. J. Schuss, M. Porkolab, Y. Takase, D. Cope, S. Fairfax, M. Greenwald, D. Gwinn, I. H. Hutchinson, B. Kusse, E. Marmar, D. Overskei, D. Pappas, R. R. Parker, L. Scaturro, J. West and S. Wolfe, *Nucl. Fusion* **21**, 427 (1981).

[2]C. M. Surko, R. E. Slusher, J. J. Schuss, R. R. Parker, I. H. Hutchinson, D. Overskei, and L. S. Scaturro, *Phys. Rev. Lett.* **43**, 1016 (1979); R. E. Slusher, C. M. Surko, J. J. Schuss, R. R. Parker, I. H. Hutchinson, D. Overskei, and L. S. Scaturro, *Phys. Fluids* **25**, 457 (1982).

[3]Y. Takase, M. Porkolab, and J. J. Schuss, *Bull. Am. Phys. Soc.* **27**, 1103 (1982).

[4]R. L. Watterson, Y. Takase, M. Porkolab, J. J. Schuss, R. E. Slusher and C. M. Surko, presented at the Fifth Topical Conference on Radio Frequency Plasma Heating, Madison, Wisconsin, 21-23 Feb. 1983, paper A-L.4 (to be published).

[5]P. T. Bonoli and E. Ott, *Phys. Rev. Lett.* **46**, 424 (1981); P. T. Bonoli and E. Ott, *Phys. Fluids* **25**, 359 (1982).

[6]P. L. Andrews and F. W. Perkins, *Bull. Am. Phys. Soc.* **26**, 1033 (1981).

[7]M. Porkolab, *Phys. Fluids* **17**, 1432 (1974).

[8]J. F. Drake, P. K. Kaw, Y. C. Lee, G. Schmidt, C. S. Liu and M. N. Rosenbluth, *Phys. Fluids* **17**, 778 (1974).

[9]M. Porkolab, *Phys. Fluids* **20**, 2058 (1977).

[10]P. M. Bellan and M. Porkolab, *Phys. Fluids* **23**, 96 (1974).

[11]J. Stevens, M. Ono, R. Horton and J. R. Wilson, *Nucl. Fusion* **21**, 1259 (1981).

[12]M. Porkolab, J. Schuss, Y. Takase, K. I. Chen, S. Knowlton, S. Luckhardt and S. McDermott, in *Heating in Toroidal Plasmas*, EUR 7424 EN, I, 355 (1980) [Proc. 2nd Joint Varenna-Grenoble Int. Symp., Villa Olmo, Como, Italy, 3 Sept. 1980]; also, M. Porkolab, J. J. Schuss, Y. Takase, S. Texter, C. L. Fiore, R. Gandy, M. J. Greenwald, D. A. Gwinn, B. Lipschultz, E. S. Marmar, D. S. Pappas, R. R. Parker, J. E. Rice, J. L. Terry, S. M. Wolfe, S. F. Knowlton, K. I. Chen, S. C. Luckhardt, M. J. Mayberry, P. T. Bonoli, B. Coppi, and R. Englade, in *Heating in Toroidal Plasmas*, EUR 7979 EN, II, 469 (1982) [Proc. 3rd Joint Varenna-Grenoble Int. Symp., Grenoble, France, 22 March 1982].

[13]K. L. Wong, J. R. Wilson and M. Porkolab, *Phys. Fluids* **23**, 96 (1980).

[14]K. L. Wong and M. Ono, *Phys. Rev. Lett.* **47**, 842 (1981).

[15]E. Villalon and A. Bers, *Nucl. Fusion* **20**, 243 (1980).

[16]M. Porkolab, in *Fusion* (Ed. E. Teller), Academic Press, 1B, 165 (1981).

[17]T. H. Stix, *The Theory of Plasma Waves*, McGraw-Hill, New York (1962).

[18]J. J. Thomson, W. L. Kruer, S. E. Bodner, and J. S. DeGroot, *Phys. Fluids* **17**, 849 (1974); J. J. Thomson and J. I. Karush, *Phys. Fluids* **17**, 1608 (1974); J. J. Thomson, *Nucl. Fusion* **15**, 237 (1975).

[19]S. P. Obenschain, N. C. Luhmann, Jr., and P. T. Greiling, *Phys. Rev. Lett.* **36**, 1309 (1976).

[20]G. Laval, R. Pellat, and D. Pesme, *Phys. Rev. Lett.* **36**, 192 (1976); G. Laval, R. Pellat, D. Pesme, A. Ramani, M. N. Rosenbluth, and E. A. Williams, *Phys. Fluids* **20**, 2049 (1977); E. A. Williams, J. R. Albritton, and M. N. Rosenbluth, *Phys. Fluids* **22**, 139 (1979).

[21]L. Chen and R. L. Berger, *Nucl. Fusion* **17**, 779 (1977).

[22]F. Y. F. Chu and C. F. F. Karney, *Phys. Fluids* **20**, 1728 (1977).

[23]K. Uehara and T. Nagashima, in *Heating in Toroidal Plasmas*, II, 485 (1982) [Proc. 3rd Joint Varenna-Grenoble Int. Symp., Grenoble, France, 22 March 1982].

[24]J. E. Stevens, S. Bernabei, M. Bitter, F. Boody, N. Bowen, A. Cavallo, T. K. Chu, S. Cohen, P. Colestock, S. Davis, C. Daughney, F. Dylla, P. Efthimion, D. Herndon, E. Hinnov, W. Hooke, J. Hosea, J. Hovey, H. Hsuan, D. Hwang, D. Ignat, F. Jobes, R. Kaita, J. Lawson, A. Martin, E. Mazzucato, D. McNeill, S. Medley, E. Meservey, R. Motley, D. Mueller, D. Ruzic, J. Schivell, F. Schnabl, R. Schwartz, J. Strachan, S. Suckewer, S. Von Goeler, and R. Wilson, in *Heating in Toroidal Plasmas*, II, 455 (1982) [Proc. 3rd Joint Varenna-Grenoble Int. Symp., Grenoble, France, 22 March 1982].

[25]S. C. Luckhardt, M. Porkolab, K. I. Chen, A. S. Fisher, F. S. McDermott and M. J. Mayberry, *Phys. Rev. Lett.* 48, 152 (1982).

[26]C. Gormezano, P. Blanc, M. El Shaer, W. Hess, G. Ichtchenko, R. Magne, G. Melin, D. Moulin, P. O'Connor, G. W. Pacher, H. D. Pacher, F. Soeldner, G. Tonon and J. G. Wegrowe, in *Heating in Toroidal Plasmas*, II, 439 (1982) [Proc. 3rd Joint Varenna-Grenoble Int. Symp., Grenoble, France, 22 March 1982].

TABLE I — Examples of thresholds due to finite growth region in the x-direction for accessible $n_{0\parallel}$ discussed in Section IV–A. The convective threshold electric fields $E^{conv}_{0\parallel th}$ calculated from Eq. (25) are shown. The homogeneous (collisional) thresholds $E^{hom}_{0\parallel th}$ given by Eq. (14) are also shown for comparison. T_i was assumed to be equal to T_e.

	$n_e(\text{cm}^{-3})$	T_e(eV)	$n_{0\parallel}$	$n_{\parallel}^{-}$	$E^{hom}_{0\parallel th}$(kV/cm)	$E^{conv}_{0\parallel th}$(kV/cm)
Alcator A[a]	4×10^{11}	3	2	5	0.03	>10
			2	20		4
Alcator C[b]	5×10^{12}	5	3	5	0.12	4
			3	20		0.6
800MHz expt.[c]	2×10^{11}	10	5	7	0.015	0.6
			5	20		0.15

[a] $P_{RF} = 1$kW corresponds to $E_{WG} = 0.33$kV/cm. $L_z = 2.6$cm, $L_y = 8.1$cm.

[b] $P_{RF} = 1$kW corresponds to $E_{WG} = 0.15$kV/cm. $L_z = 3.8$cm, $L_y = 23$cm.

[c] $P_{RF} = 1$kW corresponds to $E_{WG} = 0.09$kV/cm. $L_z = 12$cm, $L_y = 25$cm.

FIGURE CAPTIONS

FIGURE 1 — The coordinate system used in the present calculations. In region A a standing wave is formed in the z-direction.

FIGURE 2 — $\omega_R/k_{\|}v_{ti}$ (circles) and $\gamma/k_{\|}v_{ti}$ (triangles) as a function of RF power obtained from Eq. (1). The solid curves correspond to the reactive quasi-mode scaling Eqs. (10) and (11). The parameters used are: Alcator A, deuterium plasma, $B = 5\text{T}$, $n_e = 4 \times 10^{11}\text{cm}^{-3}$, $T_e = T_i = 3\text{eV}$, $ck_{0\|}/\omega_0 = 2$ and $ck_{\|}/\omega_0 = 7$.

FIGURE 3 — Contour plot of $\log_{10}|\chi_{iIm}/\chi_{eIm}|$ as a function of $\omega_R/k_{\|}v_{ti}$ and $\gamma/k_{\|}v_{ti}$. Alcator A parameters: deuterium plasma, $B = 5\text{T}$, $n_e = 1 \times 10^{12}\text{cm}^{-3}$, $T_e = T_i = 3\text{eV}$, $ck_{0\|}/\omega_0 = 2$ and $ck_{\|}/\omega_0 = 7$.

FIGURE 4(a) — A numerical solution of Eq. (1). ω_R/ω_0(solid line) and γ/ω_0(broken line) are plotted against $k\lambda_{De}$. The parameters are: Alcator A, deuterium plasma, $B = 5\text{T}$, $n_e = 4 \times 10^{11}\text{cm}^{-3}$, $T_e = T_i = 3\text{eV}$, $P_{RF} = 10\text{kW}$, $ck_{0\|}/\omega_0 = 2$ and $ck_{\|}/\omega_0 = 7$.

FIGURE 4(b) — γ/ω_0 vs. ω_R/ω_0 for the same conditions as Fig. 4(a).

FIGURE 5(a) — ω_R/ω_0(circles) and γ/ω_0(triangles) vs. radial position for Alcator A, deuterium plasma, $B = 5\text{T}$, $P_{RF} = 10\text{kW}$, $ck_{0\|}/\omega_0 = 2$ and $ck_{\|}/\omega_0 = 7$. The solid lines show the case with both $\mathbf{E} \times \mathbf{B}$ and $E_{\|}$ coupling terms and the broken lines show the case without the $\mathbf{E} \times \mathbf{B}$ coupling term. The WKB approximation is not valid in the shaded region ($r/a \gtrsim 1.2$). The assumed density and temperature profiles are shown in the inset. The arrows indicate the radial locations of the limiter, the virtual (secondary) limiter, the waveguide mouth and the vacuum chamber wall.

FIGURE 5(b) — ω_R/ω_0(circles) and γ/ω_0(triangles) vs. $ck_{||}/\omega_0$ for Alcator A, deuterium plasma, $B = 5$T, $n_e = 4 \times 10^{11}\text{cm}^{-3}$, $T_e = T_i = 3$eV, $P_{RF} = 10$kW and $ck_{0||}/\omega_0 = 2$.

FIGURE 5(c) — ω_R/ω_0(circles) and γ/ω_0(triangles) vs. RF power for Alcator A, deuterium plasma, $B = 5$T, $n_e = 4 \times 10^{11}\text{cm}^{-3}$, $T_e = T_i = 3$eV, $ck_{0||}/\omega_0 = 2$ and $ck_{||}/\omega_0 = 7$. The arrow indicates the value of $k_{||}v_{ti}/\omega_0$.

FIGURE 6(a) — ω_R/ω_0(circles) and γ/ω_0(triangles) vs. radial position for Alcator C, hydrogen plasma, $B = 8$T, $P_{RF} = 40$kW, $ck_{0||}/\omega_0 = 3$ and $ck_{||}/\omega_0 = 8$. The solid lines show the case with both $\mathbf{E} \times \mathbf{B}$ and $E_{||}$ coupling terms and the broken lines show the case without the $\mathbf{E} \times \mathbf{B}$ coupling term. WKB approximation is valid at all points plotted. The assumed density and temperature profiles are shown in the inset.

FIGURE 6(b) — ω_R/ω_0(circles) and γ/ω_0(triangles) vs. $ck_{||}/\omega_0$ for Alcator C, hydrogen plasma, $B = 8$T, $n_e = 5 \times 10^{12}\text{cm}^{-3}$, $T_e = T_i = 5$eV, $P_{RF} = 40$kW and $ck_{0||}/\omega_0 = 3$.

FIGURE 6(c) — ω_R/ω_0(circles) and γ/ω_0(triangles) vs. RF power for Alcator C, hydrogen plasma, $B = 8$T, $n_e = 5 \times 10^{12}\text{cm}^{-3}$, $T_e = T_i = 5$eV, $ck_{0||}/\omega_0 = 3$ and $ck_{||}/\omega_0 = 8$. The arrow indicates the value of $k_{||}v_{ti}/\omega_0$.

FIGURE 7 — The geometry considered in Section III–A when $k_{0y} = k_{2y} = 0$. The region $|z - C_0x| \leq L_z/2$ is the pump resonance cone. The sideband lower hybrid waves grow while they are in this region but they stop growing as they travel parallel to the resonance cone $|z - C_2x| \leq L_z/2$ and get out of this region. $C_0 \equiv v_{0z}/v_{0x}$ and $C_2 \equiv v_{2z}/v_{2x}$.

FIGURE 8 — The geometry considered in Section III–B when $k_{2y} \neq 0$. The projection on the x-y plane is shown. The z-direction points out of the paper. $C_0 \equiv v_{0y}/v_{0x}$ and $C_2 \equiv v_{2y}/v_{2x}$.

FIGURE 9 — The relative magnitudes of the components of the wavevectors $\mathbf{k}_0$, $\mathbf{k}_1$ and $\mathbf{k}_2$ considered in Section IV–A.

FIGURE 10(a) — G_0/A_0 vs. x and y for $C_0 = 0$, $C_2 = 10$, $A_0(L_y/2) = 150$ and $A_2/A_0 = 10^{-4}$.

FIGURE 10(b) — G_2/A_0 vs. x and y for the same parameters as Fig. 10(a).

FIGURE 10(c) — Pump power integrated over y vs. x for the same parameters as Fig. 10(a).

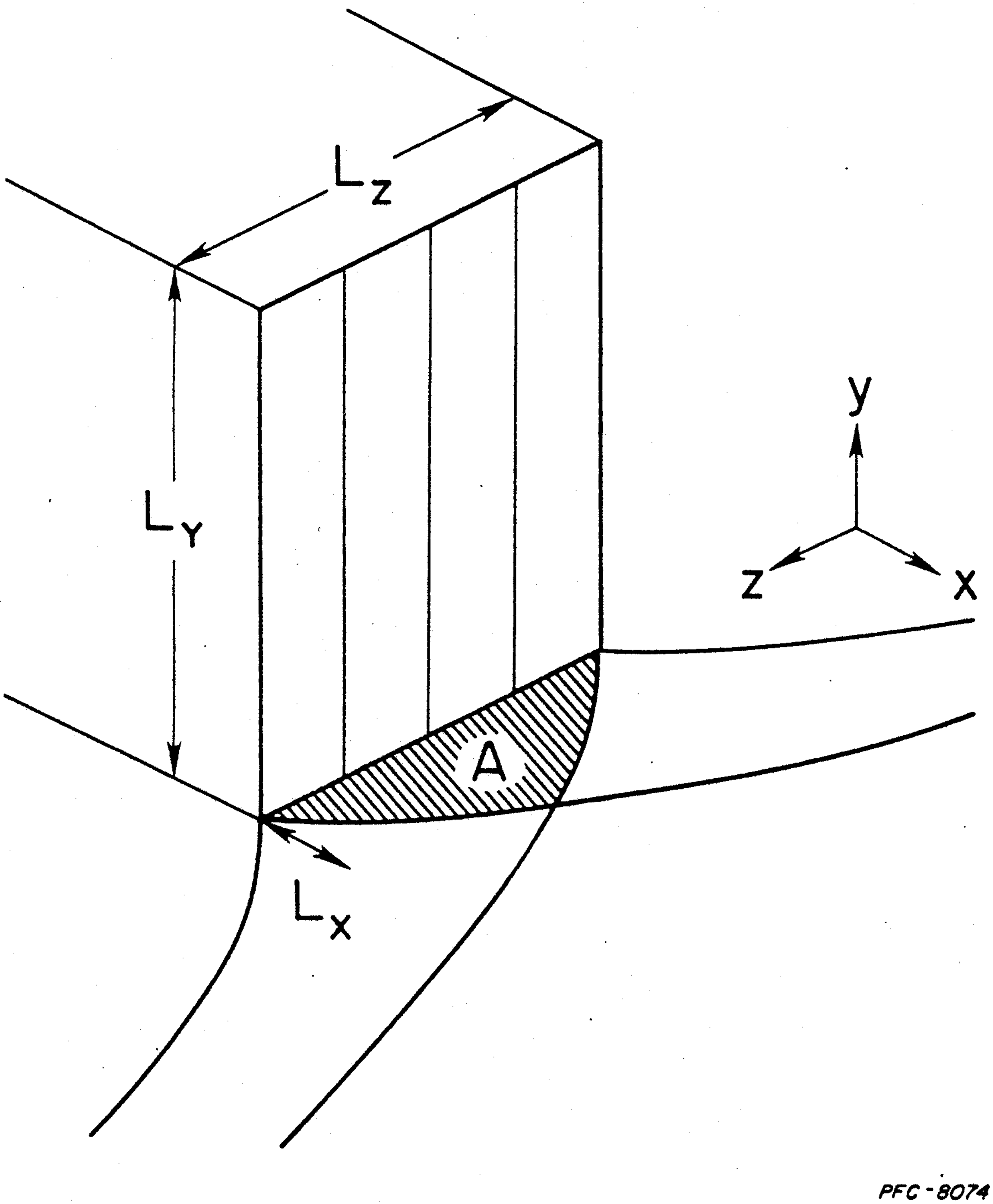

FIGURE 1

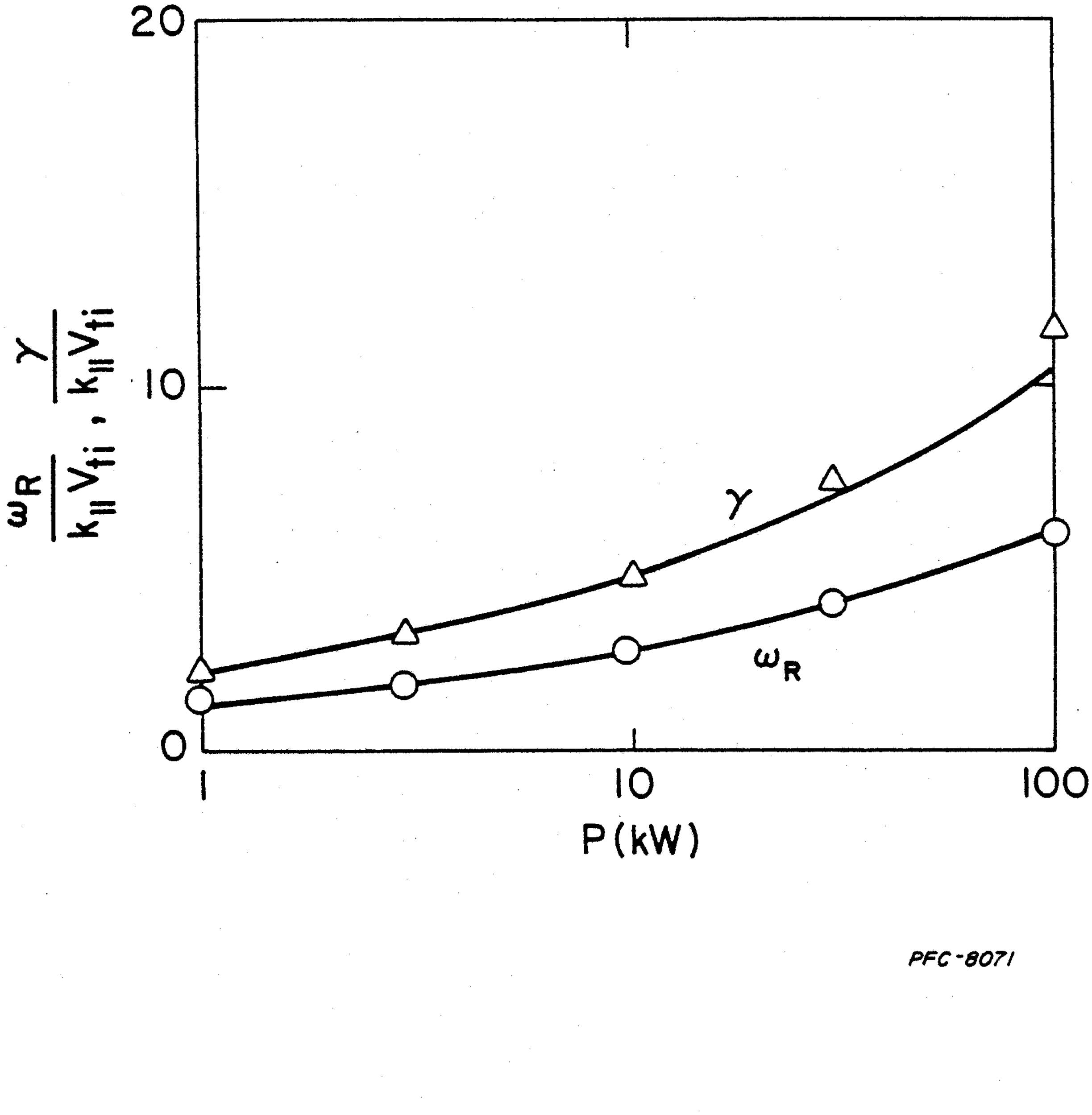

20
10
0
1
10
100
P(kW)
$\frac{\omega_R}{k_\parallel V_{ti}}$, $\frac{\gamma}{k_\parallel V_{ti}}$
γ
ω_R
PFC-8071

FIGURE 2

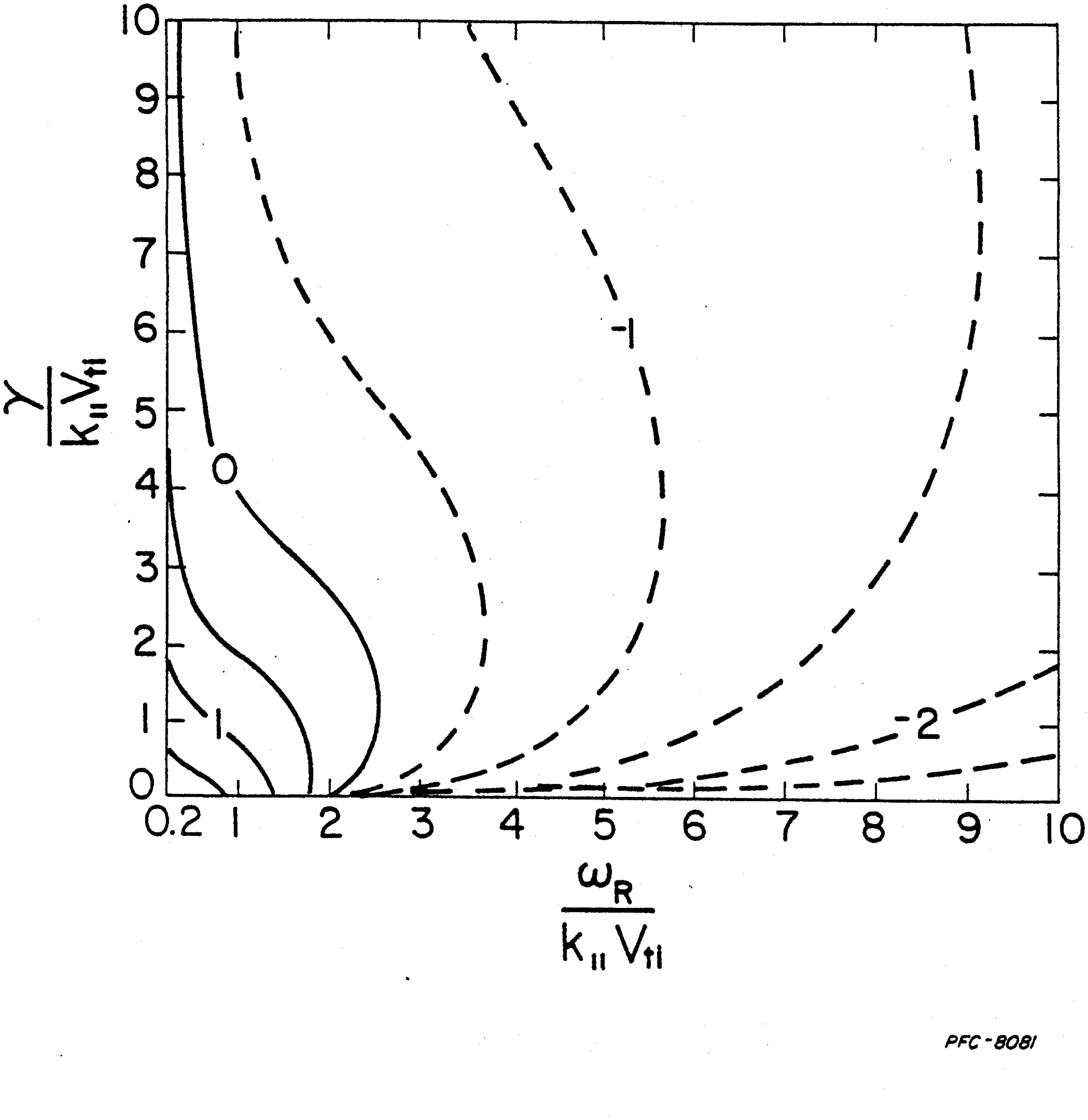
$\frac{\gamma}{k_{\parallel} V_{ti}}$
$\frac{\omega_R}{k_{\parallel} V_{ti}}$
0
1
-1
-2
0.2
PFC-8081

FIGURE 3

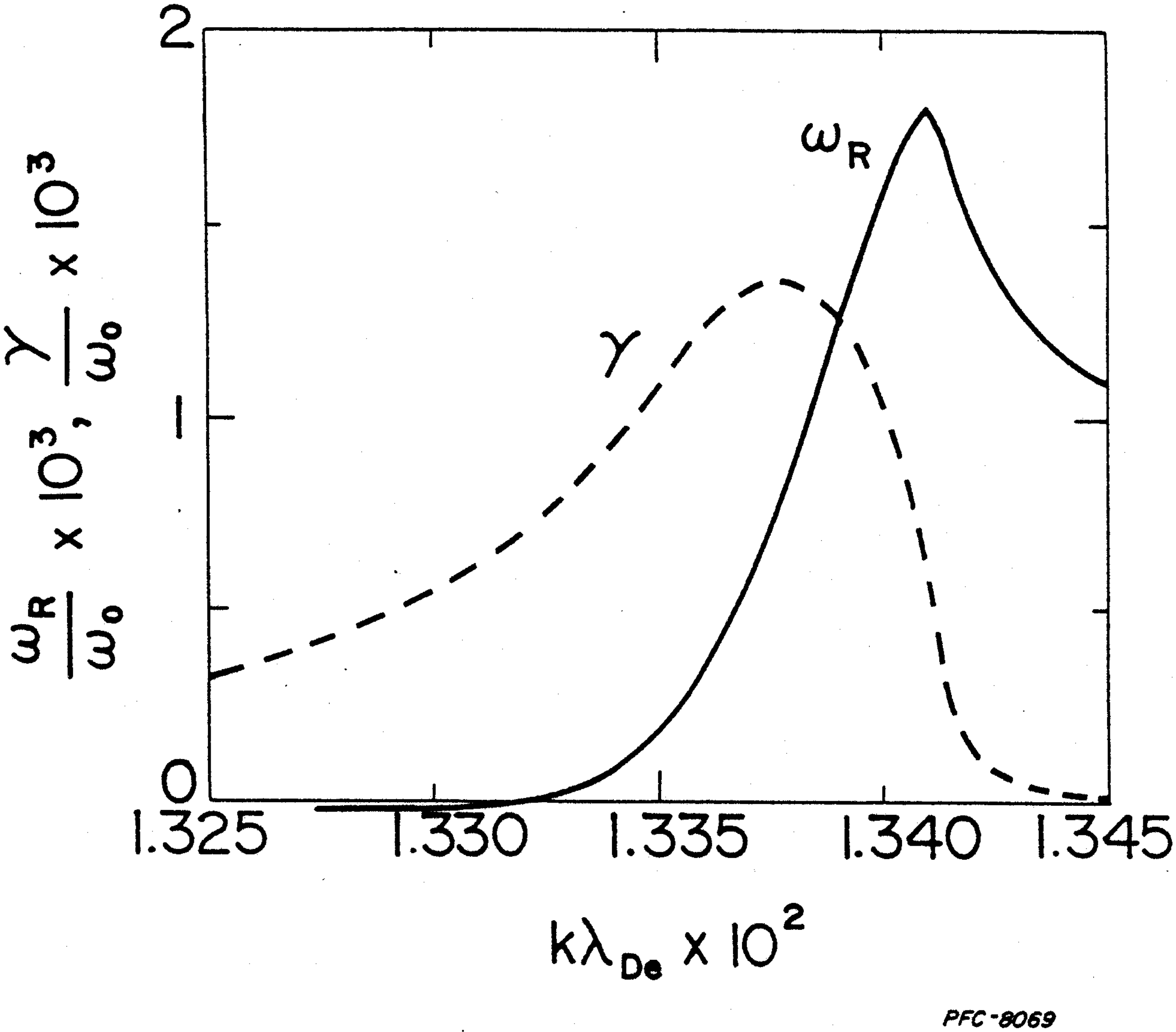

2
1
0
$\frac{\omega_R}{\omega_0} \times 10^3, \frac{\gamma}{\omega_0} \times 10^3$
ω_R
γ
1.325
1.330
1.335
1.340
1.345
$k\lambda_{De} \times 10^2$
PFC-8069

FIGURE 4(a)

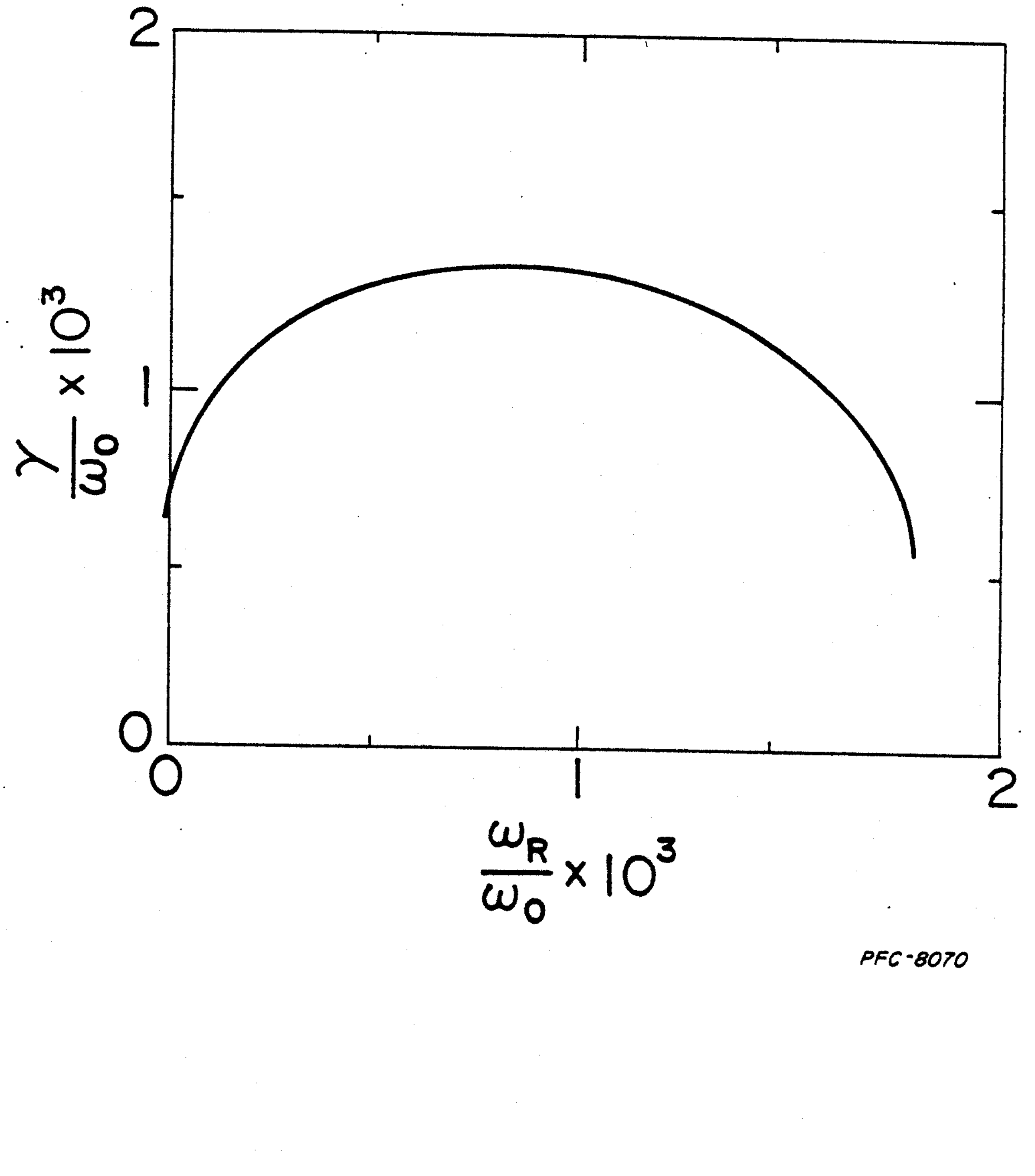
2
1
0
0
1
2
$\frac{\gamma}{\omega_0} \times 10^3$
$\frac{\omega_R}{\omega_0} \times 10^3$
PFC-8070

FIGURE 4(b)

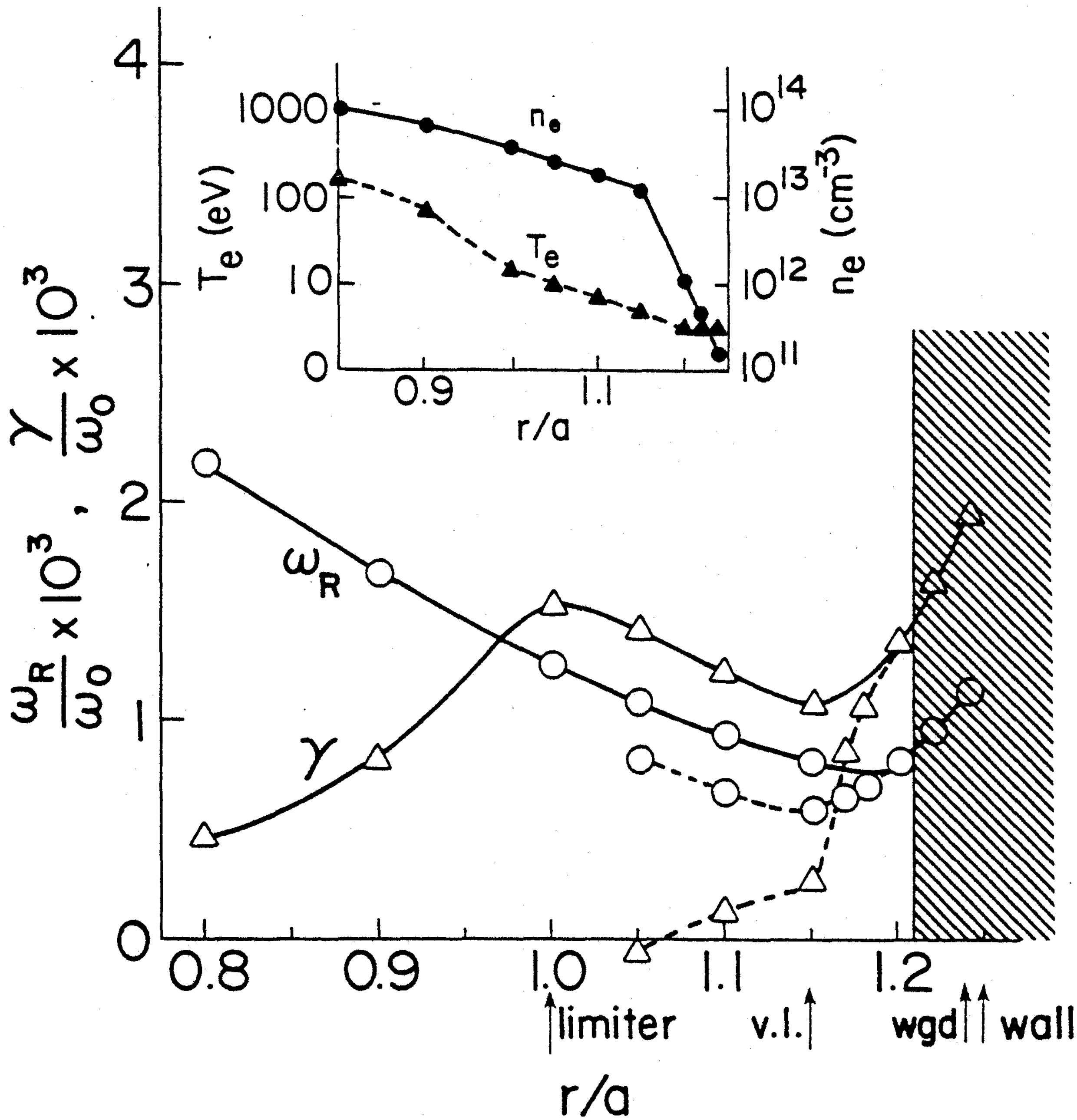

PFC-8078

FIGURE 5(a)

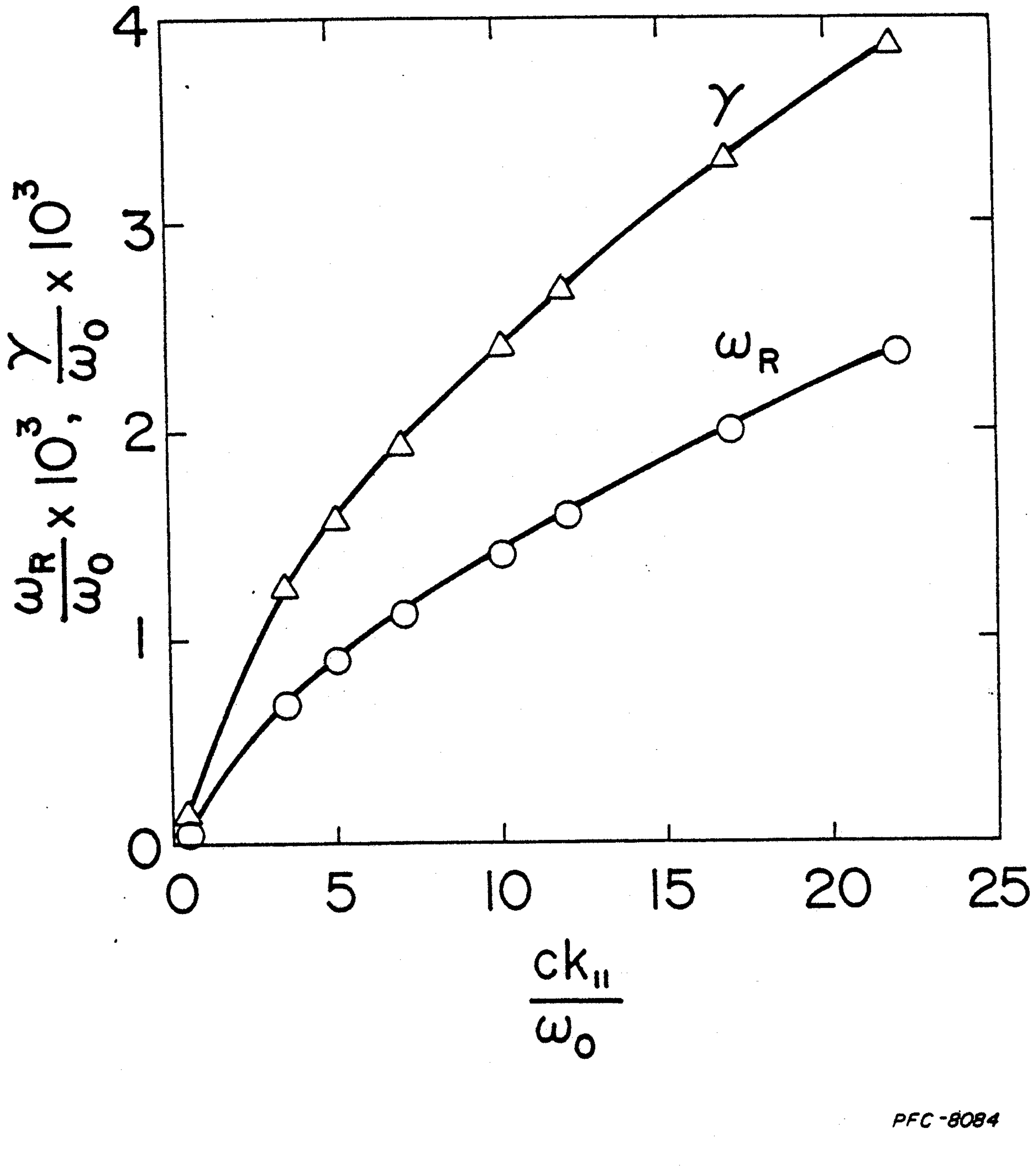

FIGURE 5(b)

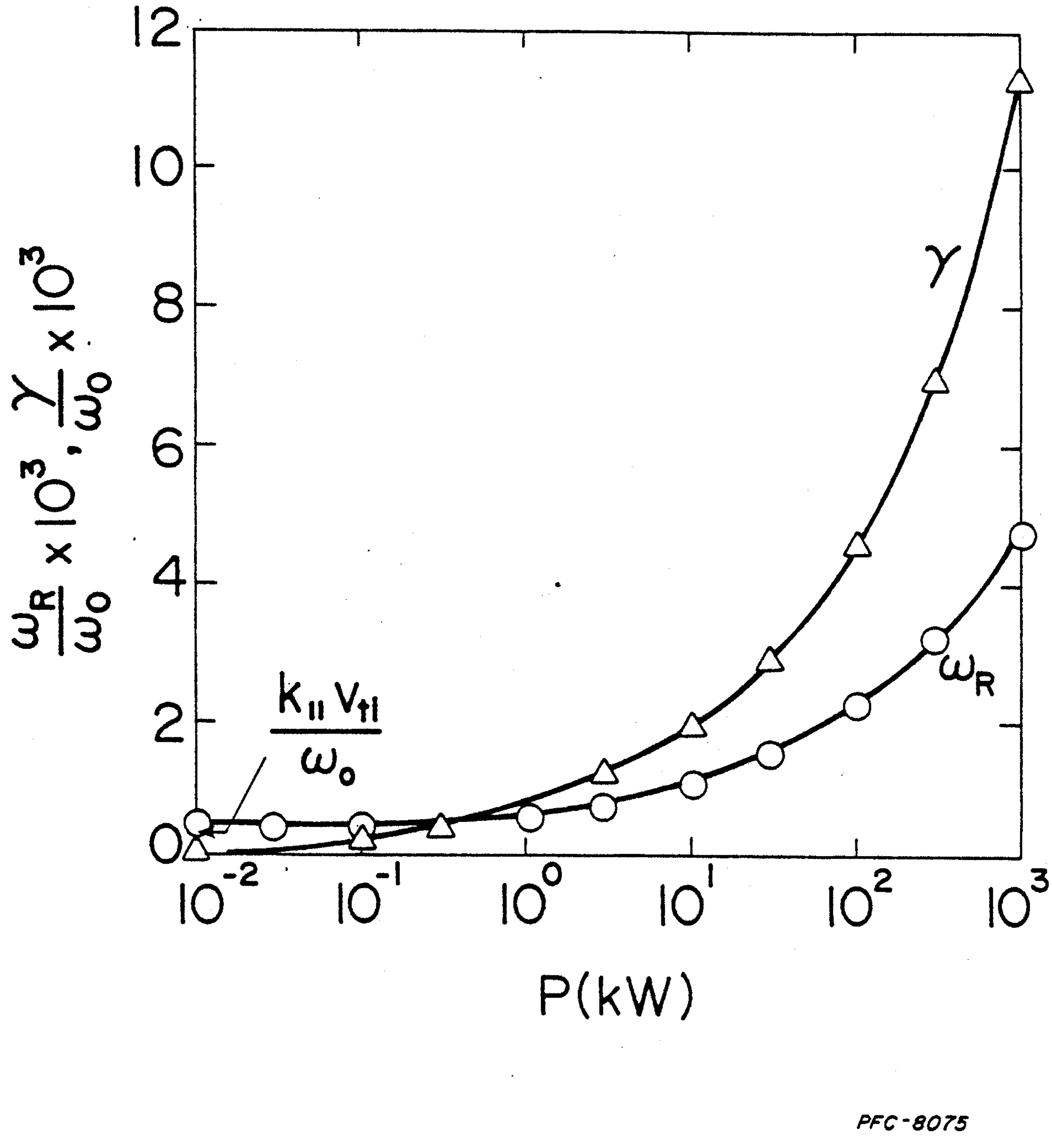

12
10
8
6
4
2
0
$\frac{\omega_R}{\omega_0} \times 10^3, \frac{\gamma}{\omega_0} \times 10^3$
γ
ω_R
$\frac{k_\parallel v_{ti}}{\omega_0}$
10^{-2}
10^{-1}
10^{0}
10^{1}
10^{2}
10^{3}
P(kW)
PFC-8075

FIGURE 5(c)

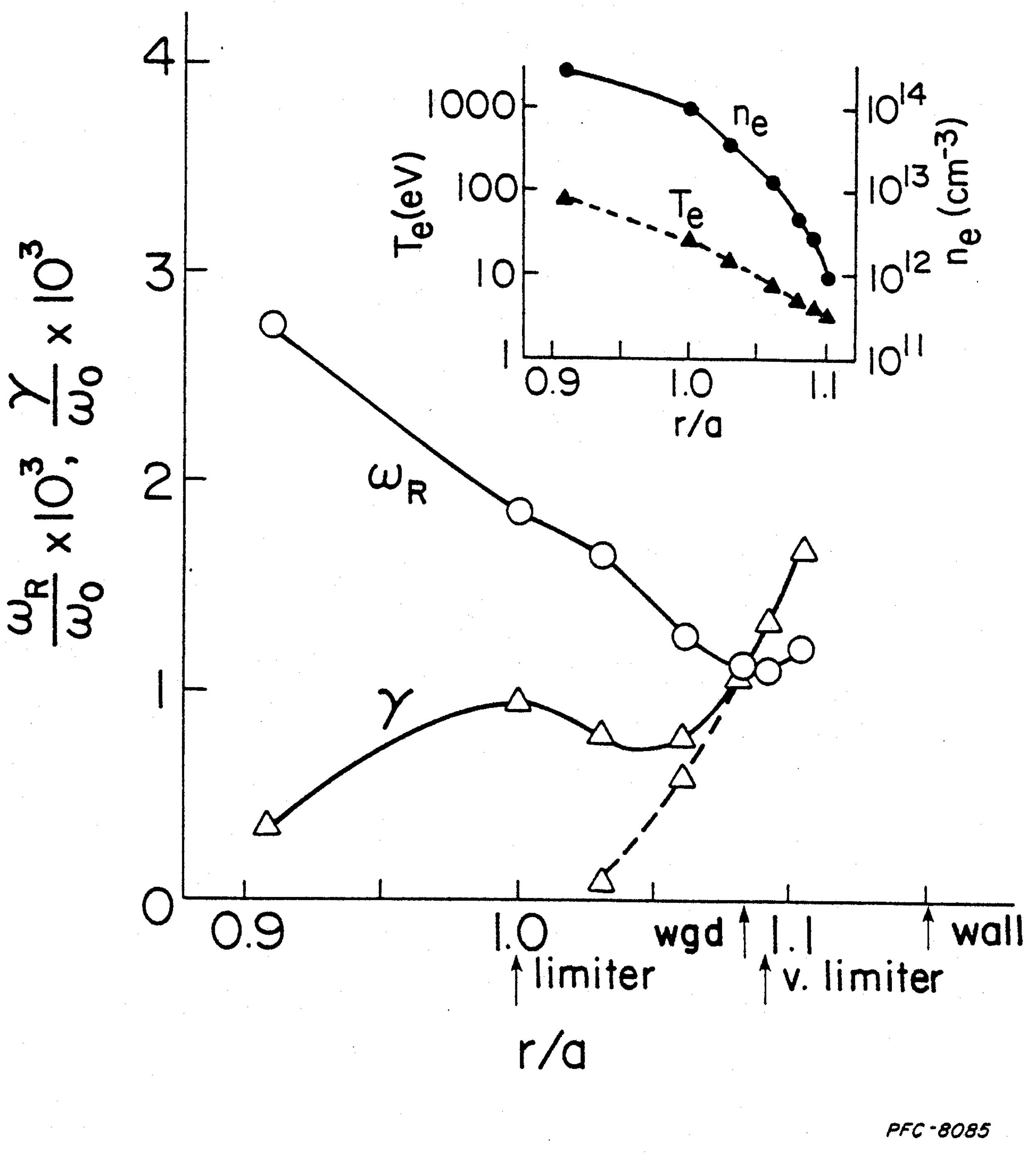

4
3
2
1
0
$\frac{\omega_R}{\omega_0} \times 10^3$, $\frac{\gamma}{\omega_0} \times 10^3$
ω_R
γ
0.9
1.0
limiter
wgd
1.1
v. limiter
wall
r/a
1000
100
10
1
T_e(eV)
n_e
T_e
10^{14}
10^{13}
10^{12}
10^{11}
n_e (cm^{-3})
0.9
1.0
1.1
r/a
PFC-8085

FIGURE 6(a)

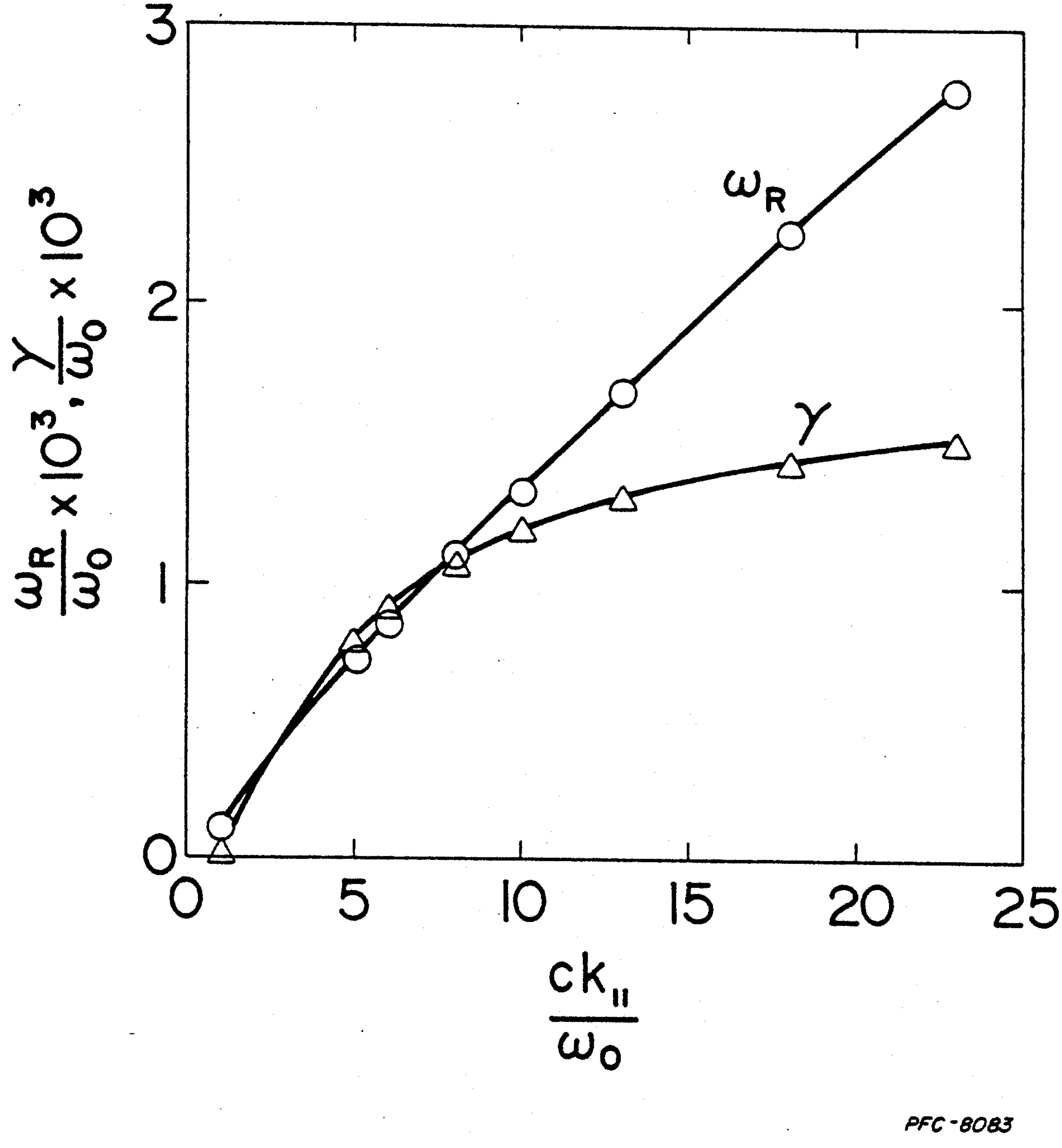

3
2
1
0
0
5
10
15
20
25
$\frac{\omega_R}{\omega_0} \times 10^3, \frac{\gamma}{\omega_0} \times 10^3$
ω_R
γ
$\frac{ck_{\parallel}}{\omega_0}$
PFC-8083

FIGURE 6(b)

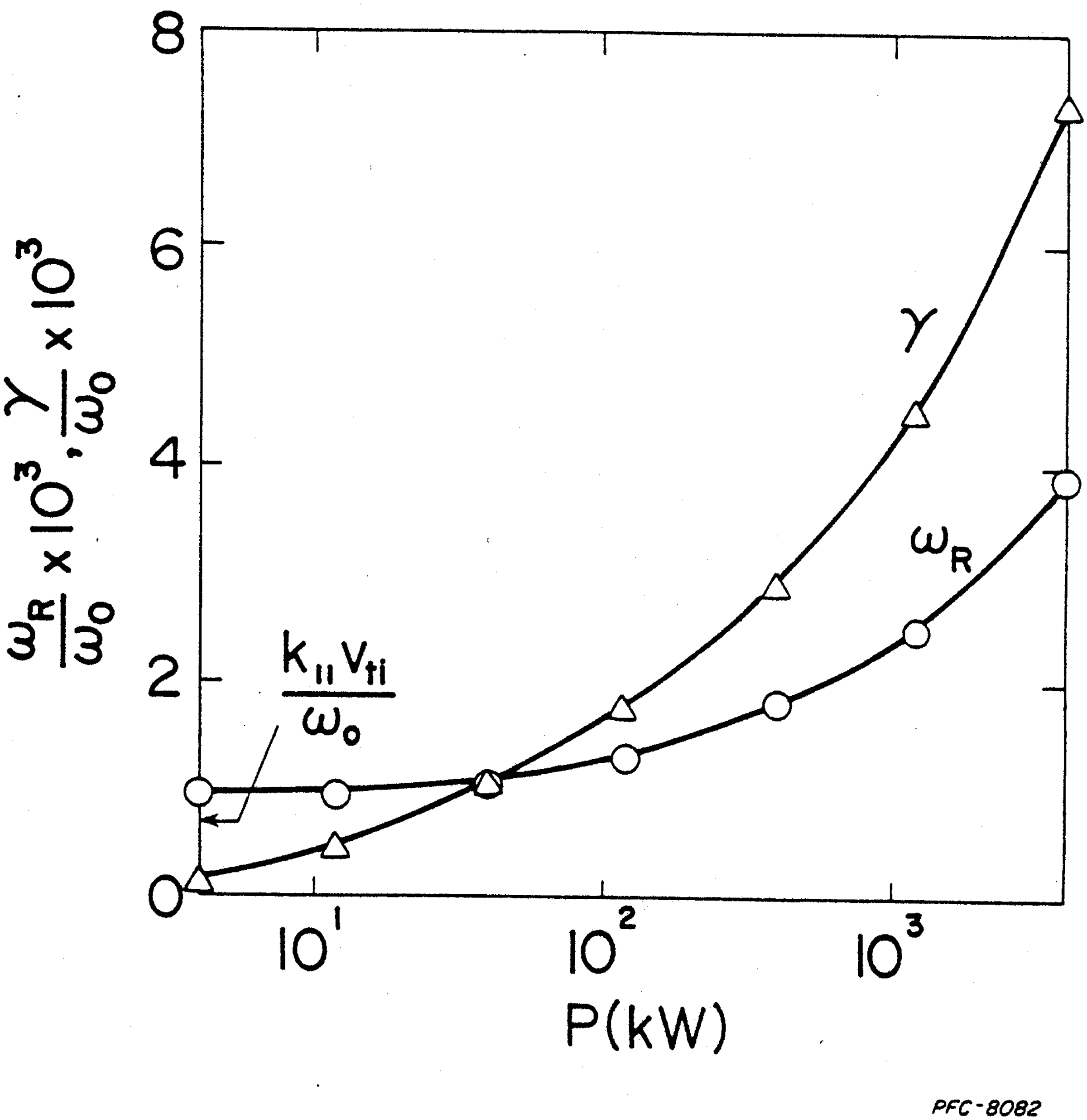

8
6
4
2
0
$\frac{\omega_R}{\omega_0} \times 10^3, \frac{\gamma}{\omega_0} \times 10^3$
γ
ω_R
$\frac{k_{\parallel} v_{ti}}{\omega_0}$
10^1
10^2
10^3
P(kW)
PFC-8082

FIGURE 6(c)

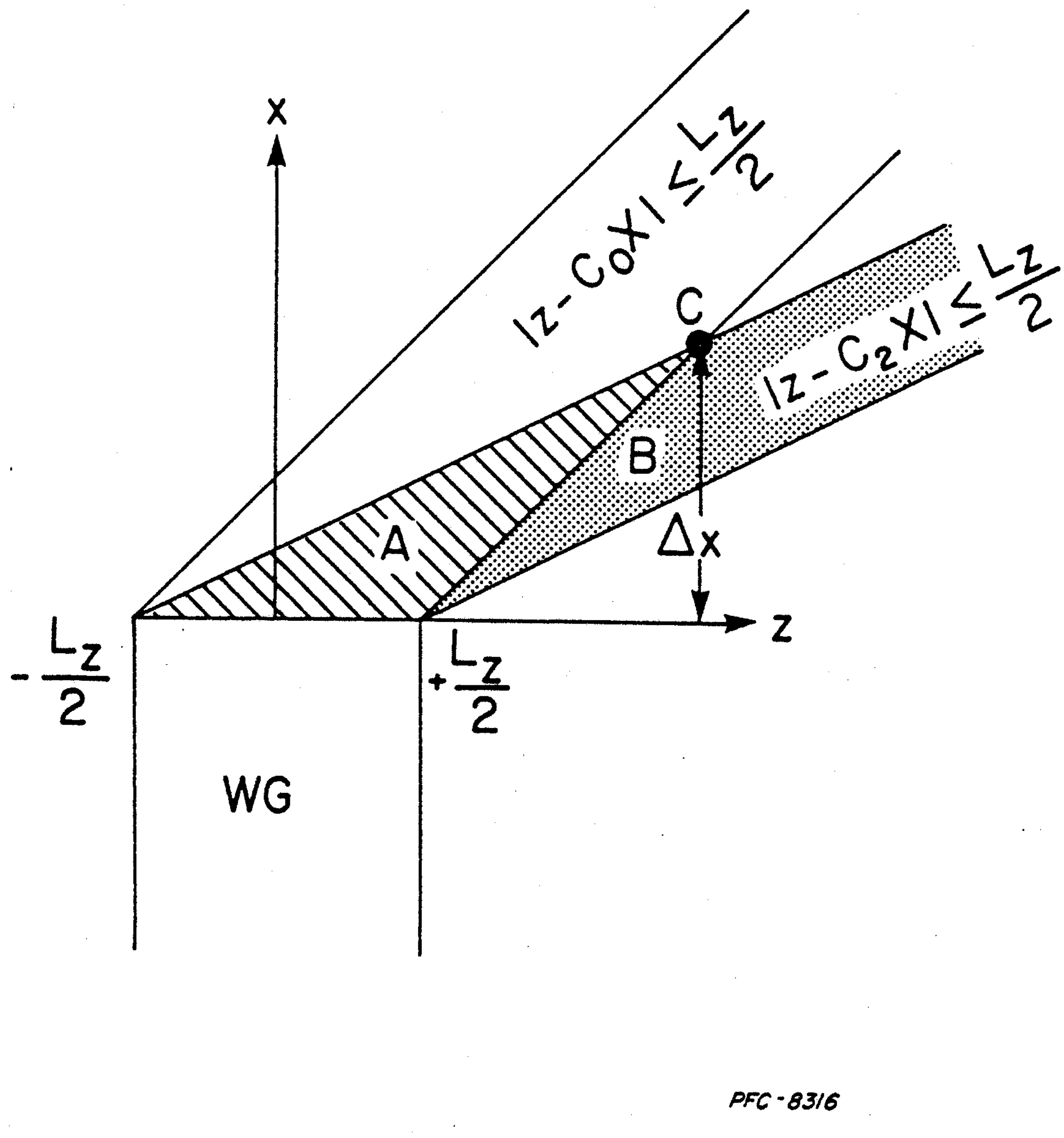
x
$|z - C_0 X| \leq L_z/2$
C
$|z - C_2 X| \leq L_z/2$
B
A
Δx
z
$-\frac{L_z}{2}$
$+\frac{L_z}{2}$
WG
PFC-8316

FIGURE 7

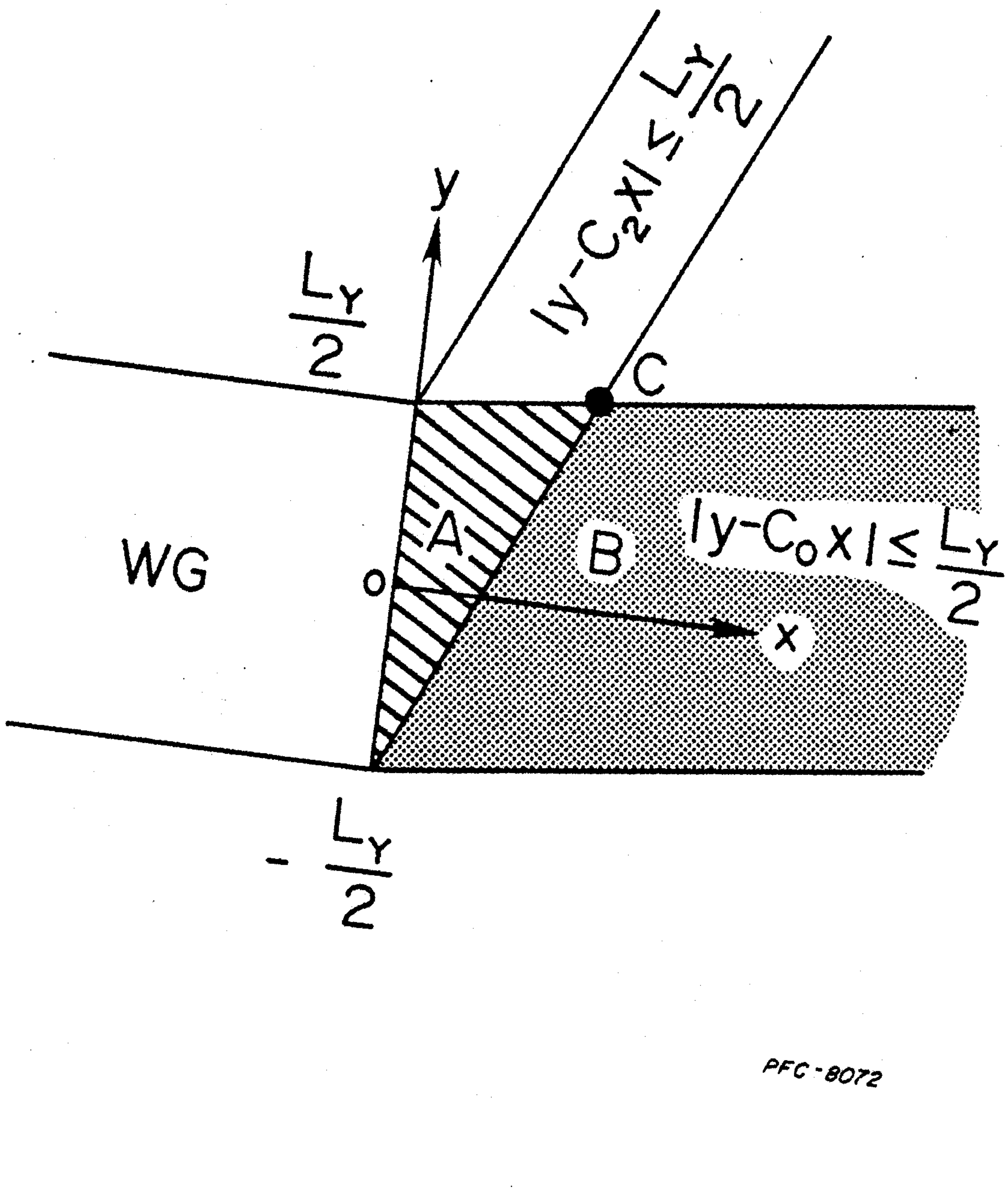
y
$|y-C_2x| \le \frac{L_Y}{2}$
$\frac{L_Y}{2}$
C
A
B
$|y-C_0x| \le \frac{L_Y}{2}$
WG
o
x
$-\frac{L_Y}{2}$
PFC-8072

FIGURE 8

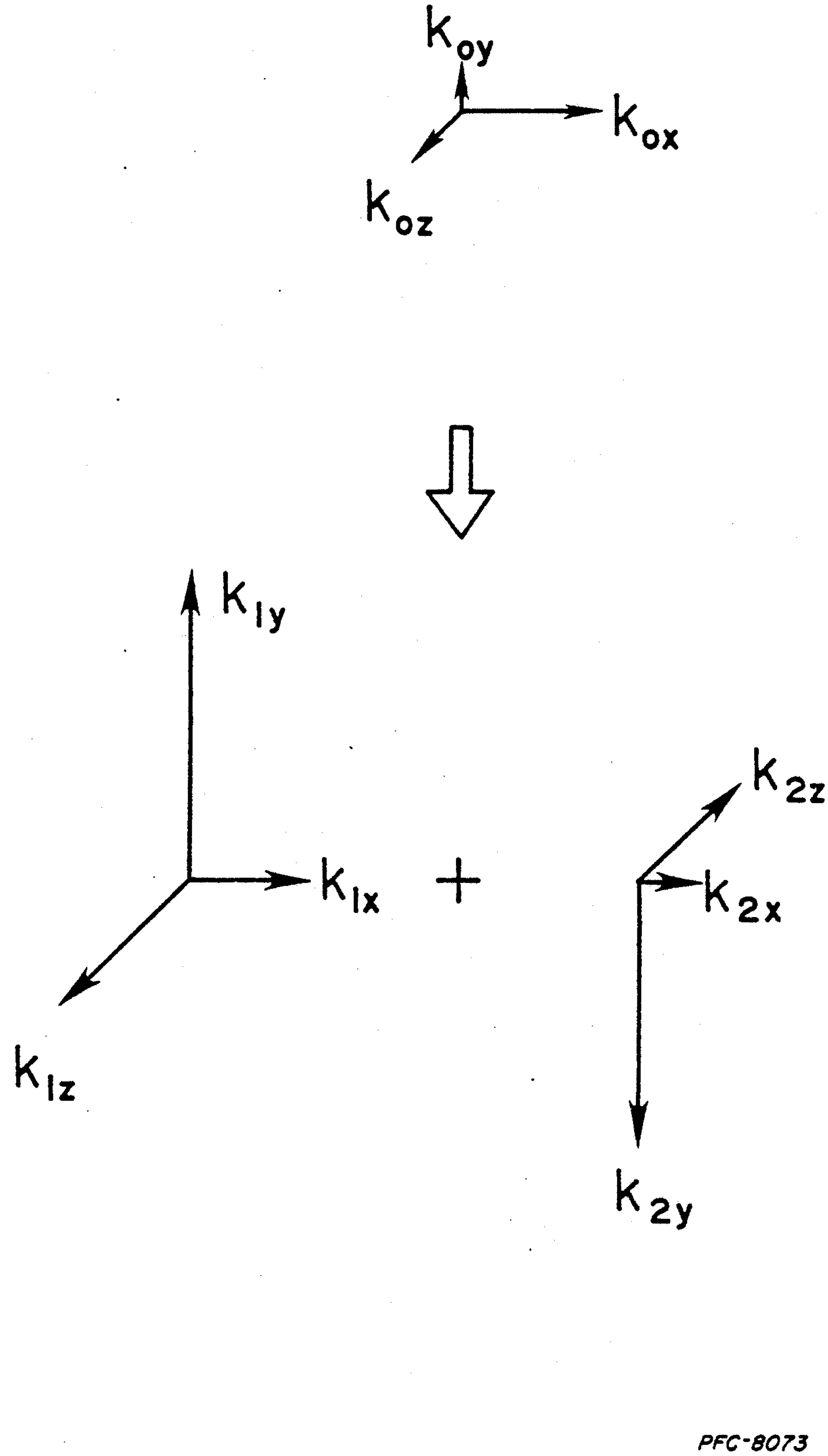

FIGURE 9

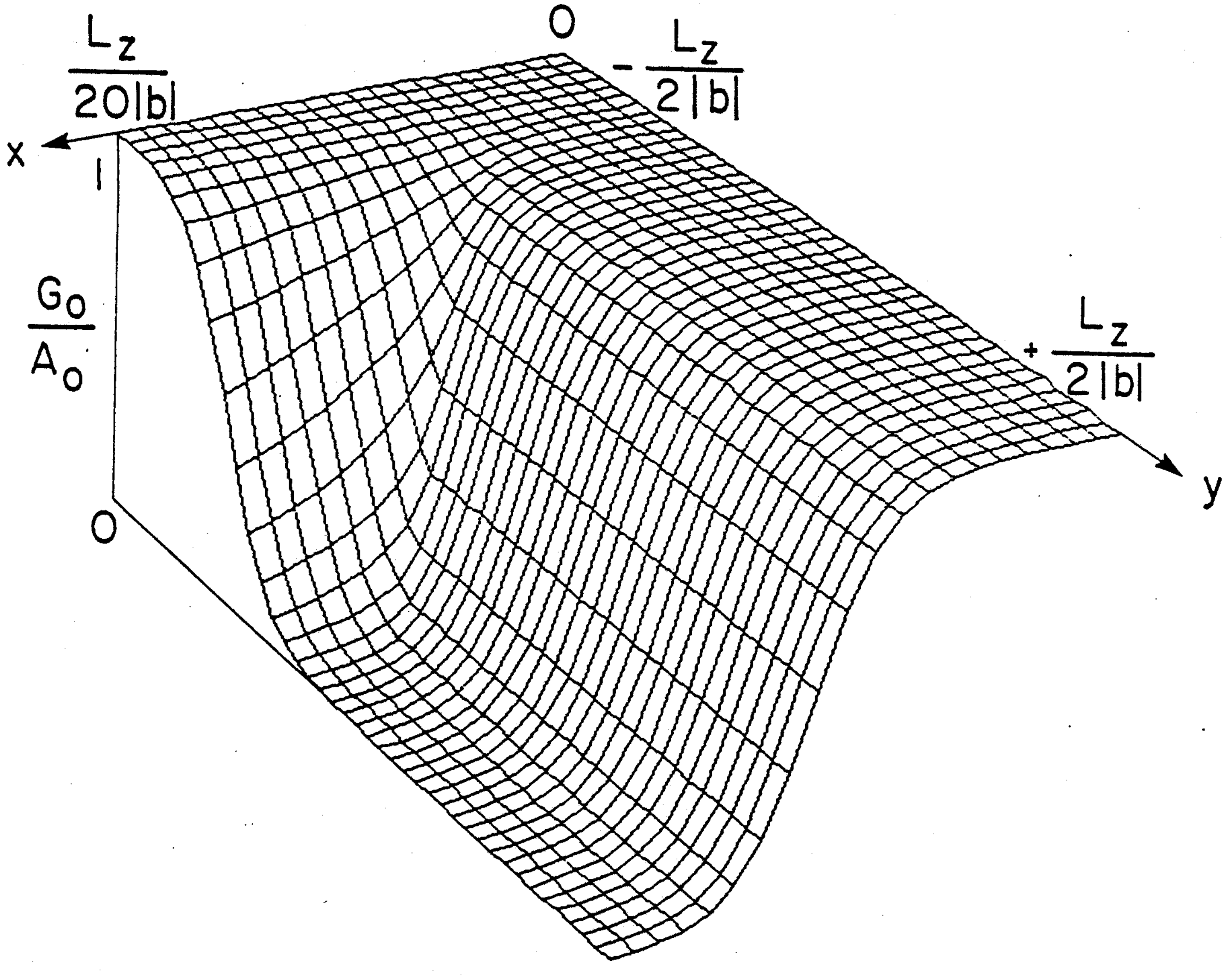

FIGURE 10(a)

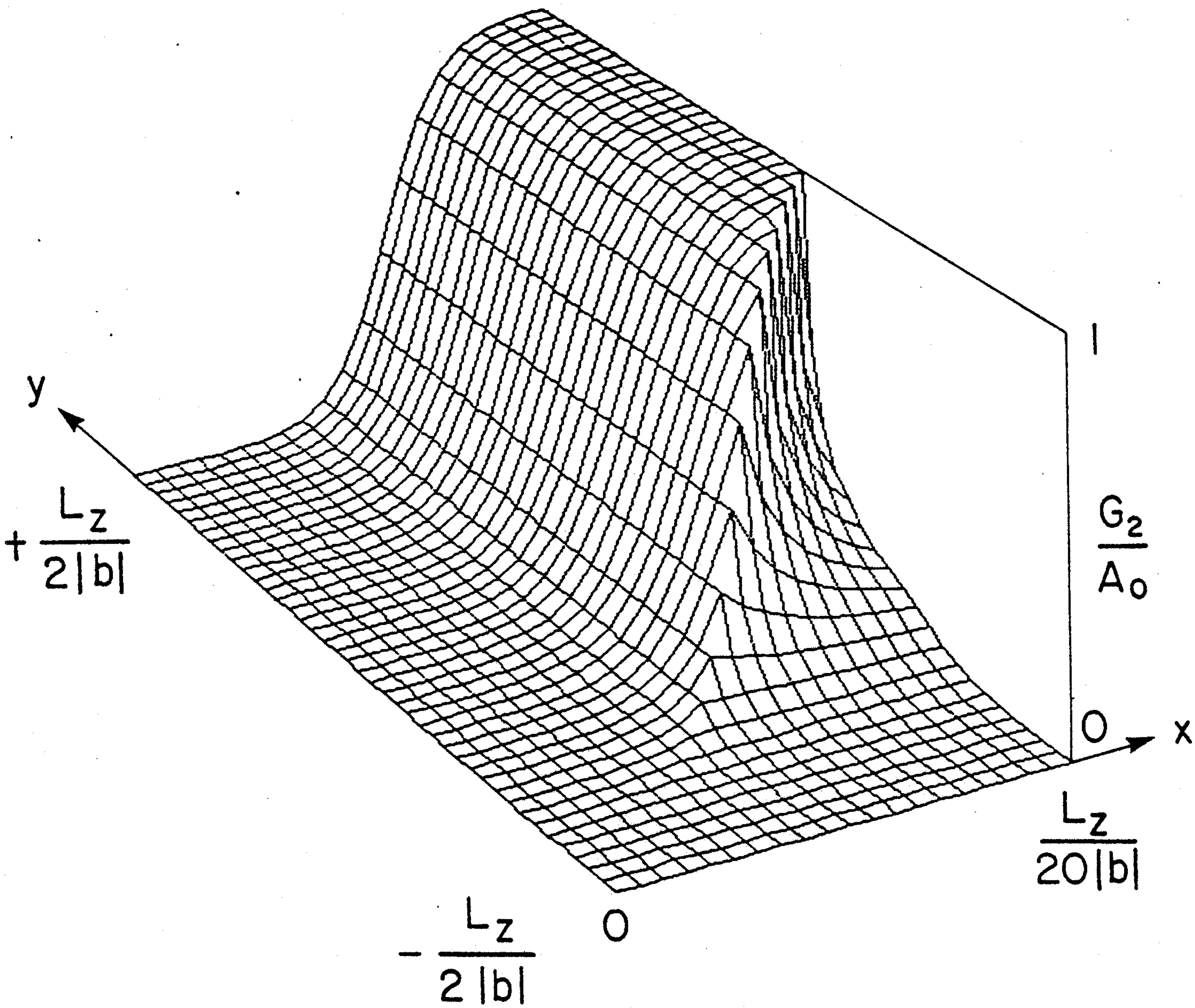

FIGURE 10(b)

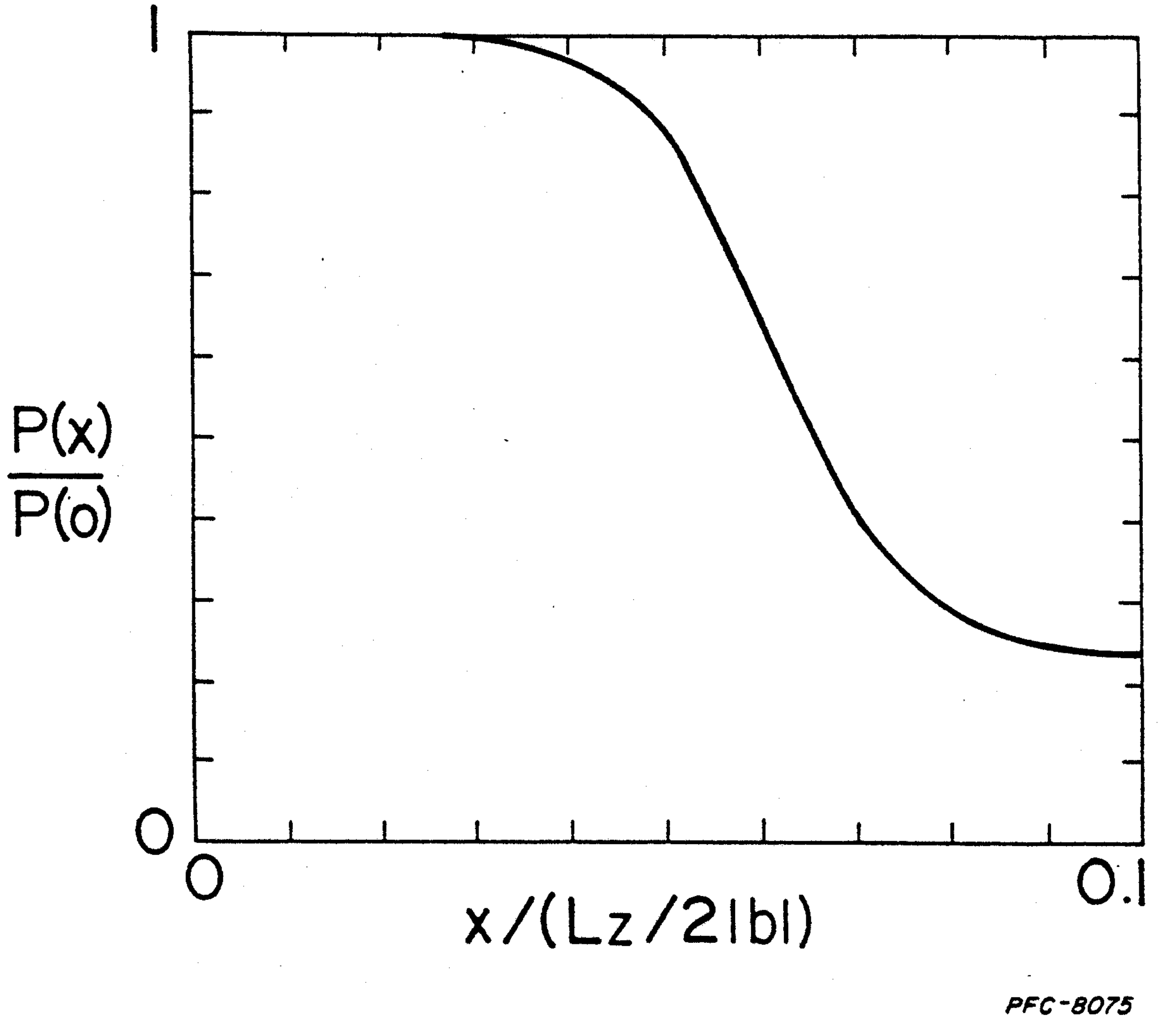

FIGURE 10(c)